Atomic Beam Frequency Standards

Richard C. Mockler

National Bureau of Standards, Radio Standards Division, Boulder, Colorado

Reprinted from

ADVANCES IN ELECTRONICS AND ELECTRON PHYSICS

Volume 15, 1961

Atomic Beam Frequency Standards

RICHARD C. MOCKLER

National Bureau of Standards, Boulder, Colorado

I. Introduction

It is natural to choose as a standard of frequency and time interval some periodic phenomenon appearing in nature that is especially uniform. The periodic rotation of the earth on its axis at one time provided a sufficiently uniform time base. As techniques of measurement improved it was demonstrated that the rotational period of the earth was slowly increasing,

an effect that has been attributed to tidal friction. In addition, there were observed irregular changes and almost periodic fluctuations in the length of the solar day. More recently (1956) astronomers have chosen the period of the orbital motion of the earth about the sun as the basis for the definition of time. This is the basis upon which time is defined (in the practical sense) today. There are secular variations in this period, but they are much more predictable than the changes in the length of the solar day. For this reason the second has been defined as 1/31,556,925.9747 of the tropical year at 12^h ET, 0 January, 1900.

Highly complex macroscopic systems such as our solar system probably are subject to some unpredictable changes and aging effects. For many purposes the periodic motions in microscopic systems of atoms would be more suitable for defining time intervals and frequency. To be sure, the separations of the quantum states of a completely isolated atom or molecule are expected to be fixed in time. The measurement of one of these separations by a suitable apparatus would provide a very excellent standard if the measurements can be made with the required precision.

Microwave and atomic beam magnetic resonance techniques provide a method of measuring state separations with probably the greatest accuracy and ease of interpretation of all the presently known spectroscopic techniques. Atomic beam techniques have the advantage that Doppler and collision broadening of the spectral line are practically eliminated. Certain atoms, especially the alkali metals, have intense spectral lines that are easily detected. Moreover, the transitions fall in a convenient range of the electromagnetic spectrum easily accessible to available coherent radiators.

A transition between the hyperfine structure (hfs) levels in the ground state of cesium provides the present working standard of frequency for the United States (*1*), the United Kingdom (*2*), Canada (*3*), and Switzerland (*4*). This transition can be measured with the remarkable precision of ± 2 parts in 10^{12}, and with an accuracy of ± 1.7 parts in 10^{11}.[1] It appears that even further improvements in precision and accuracy can be expected in the near future.

The frequency of the $(F = 4, m_F = 0) \leftrightarrow (F = 3, m_F = 0)$ transition in cesium has been measured in terms of the Ephemeris Second—the standard unit of time obtained through astronomical observations. This frequency is 9192631770 ± 20 cps (*5*). The probable error, ± 20 cps (or 2×10^{-9}), arises because of experimental limitations on the astronomical measurements and on long distance frequency comparisons. The astronomical data used in arriving at this figure were accumulated over a period of three years. A longer measurement time would reduce the probable error.

[1] Hereafter relative precisions and accuracies shall be written in the form 2×10^{-10}, for example. This has the meaning of 2 parts in 10^{10}.

With this relationship between astronomical time and the hfs separation of cesium, atomic frequency standards together with proper summing devices for counting equally spaced events can now make astronomical time immediately available, although even a temporary lapse in the summing device will irrecoverably lose the epoch at which the count was started. The long delays previously required to determine and publish the corrections to the propagated time signals are no longer necessary. Atomic time is also available with its greater uniformity. On the atomic time scale A.1 introduced by Markowitz (*5*) of the U.S. Naval Observatory, The frequency of cesium is assumed to be 9192631770.0 cps for atomic time. That is, there are that many cycles in one second of atomic time.

The present article deals primarily with cesium atomic beam frequency standards. It is not purported to be an exhaustive review. Its purpose is to provide: (a) some background in atomic beam spectroscopy in view of the fact that the area of atomic beam frequency standards is no longer solely of interest to the physicist,[2] (b) some design considerations of atomic beam standards, and (c) results of comparisons between various cesium standards.

The Introduction is followed by a description of the spectrum upon which the cesium standard is based (Sections II, III, and IV). Section V describes the beam apparatus and the salient features of its design. Section VI is a discussion of the excitation process. Inaccuracies in atomic beam measurements are considered in Section VII. In Section VIII, various cesium standards are compared using radio transmission data. A discussion of various other types of atomic standards and new developments and possibilities in the field is found in Section IX.

II. Atomic Hyperfine Structure

The quantum transitions employed in present day atomic beam standards occur between the hyperfine levels in the ground state of the alkali metal cesium. The hyperfine splitting arises because of the interaction between the magnetic moment of the nucleus and the magnetic field produced by the valence electron at the position of the nucleus. (See Fig. 1.)

The Hamiltonian for this interaction is given by

$$\mathcal{H} = -\boldsymbol{\mu}_I \cdot \mathbf{H}_{el}, \tag{1}$$

where $\boldsymbol{\mu}_I$ is the magnetic dipole moment of the nucleus, and $\mathbf{H}_{el}$ is the magnetic field at the nucleus produced by the electron. For hydrogenlike atoms, $\mathbf{H}_{el}$ can be estimated from some simple semiclassical considerations. The complete discussion is complicated (*9*).

The field at the nucleus has a contribution from both the orbital motion

[2] See also the general references on atomic and molecular beam spectroscopy (*6*, *7*, *8*).

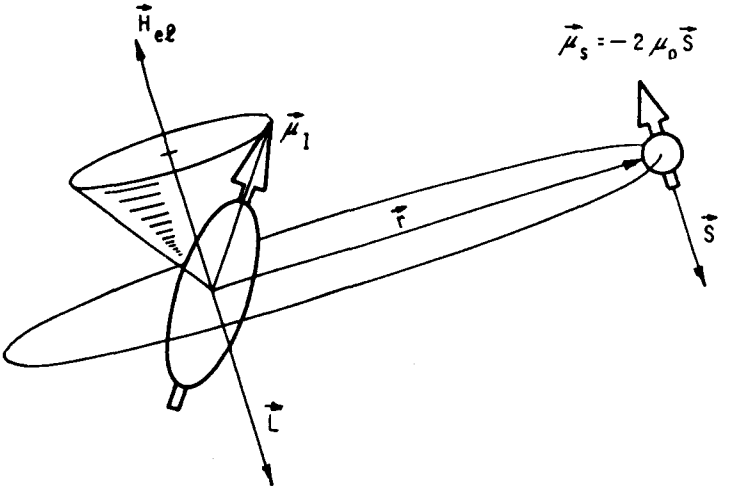

FIG. 1. Pictorial representation of the interaction of the nuclear magnetic moment with the fields produced by the orbital motion and spin of the electron.

of the electron and its intrinsic magnetic moment. Thus

$$\mathbf{H}_{el} = \mathbf{H}_{orbit} + \mathbf{H}_{spin}, \tag{2}$$

where $\mathbf{H}_{orbit}$ is the contribution from the orbital motion, and $\mathbf{H}_{spin}$ is the contribution from the spin moment. From the Biot-Savart Law,

$$\mathbf{H}_{orbit} = -\frac{e}{c}\frac{\mathbf{r}\times\mathbf{v}}{r^3} = -\frac{e}{mc}\frac{\mathbf{r}\times\mathbf{p}}{r^3}$$

or

$$\mathbf{H}_{orbit} = -\frac{e\hbar\mathbf{L}}{mcr^3} = -2\mu_0\frac{\mathbf{L}}{r^3}, \tag{3}$$

where $\mathbf{r}$ is the position vector of the electron relative to the nucleus, $\mathbf{v}$ is the velocity of the electron, $\hbar\mathbf{L}$ is the orbital angular momentum, and $\mu_0 = e\hbar/2mc$ is the Bohr magneton.

The field at the nucleus arising from the intrinsic magnetic moment of the electron can be obtained from the classical expression for the field of a dipole moment $\boldsymbol{\mu}_S = -2\mu_0\mathbf{S}$.

$$\mathbf{H}_{spin} = -\left[\frac{\boldsymbol{\mu}_S}{r^3} - \frac{3\mathbf{r}(\boldsymbol{\mu}_S\cdot\mathbf{r})}{r^5}\right] = \frac{2\mu_0}{r^3}\left[\mathbf{S} - \frac{3\mathbf{r}(\mathbf{r}\cdot\mathbf{S})}{r^2}\right], \tag{4}$$

where $\boldsymbol{\mu}_S$ is the magnetic moment of the electron.

We wish the average value of $\mathbf{H}_{el}$, and it will prove convenient to write this average as

$$\mathbf{H}_{el} = (\mathbf{H}_{el}\cdot\mathbf{J})\frac{\mathbf{J}}{J^2}, \tag{5}$$

463-560 O - 72 - 2

where $\mathbf{J} = \mathbf{L} + \mathbf{S}$. If the sum of (3) and (4) are inserted into (5),

$$\mathbf{H}_{el} = -\frac{2\mu_0}{r^3}[L^2 - S^2 + 3(\mathbf{e}_r \cdot \mathbf{S})\mathbf{e}_r(\mathbf{L} + \mathbf{S})]\frac{\mathbf{J}}{J^2}. \tag{6}$$

The unit vector $\mathbf{e}_r$ is in the direction of $\mathbf{r}$. The vectors $\mathbf{L}$ and $\mathbf{e}_r$ are perpendicular so that (6) becomes

$$\mathbf{H}_{el} = -\frac{2\mu_0}{r^3}[L^2 - S^2 + 3(\mathbf{e}_r \cdot \mathbf{S})^2]\frac{\mathbf{J}}{J^2}. \tag{7}$$

$(\mathbf{e}_r \cdot \mathbf{S})^2$ can be estimated from the vector model: $\mathbf{L}$ and $\mathbf{S}$ precess rapidly about $\mathbf{J}$ in the laboratory frame of reference. Consider the coordinate

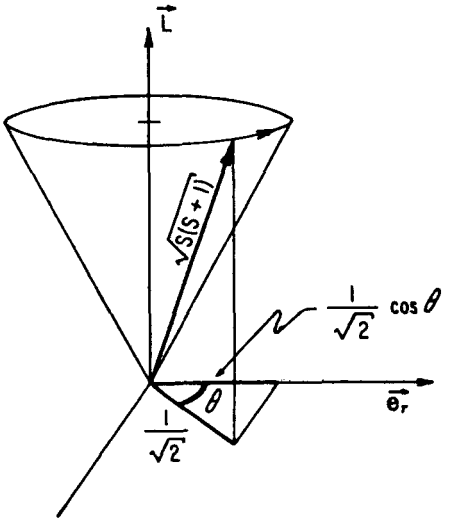

FIG. 2. Coordinate system in which $\mathbf{L}$ and $\mathbf{e}_r$ are fixed.

system in which $\mathbf{L}$ and $\mathbf{e}_r$ are fixed. In this system $\mathbf{S}$ precesses about $\mathbf{L}$ (Fig. 2). For one electron ($S = 1/2$), the average of the square of the projection of $\mathbf{S}$ on $\mathbf{e}_r$ is

$$\overline{(e_r \cdot \mathbf{S})^2} = \frac{1}{2\pi}\int_0^{2\pi}\left(\frac{1}{\sqrt{2}}\cos\theta\right)^2 d\theta = \frac{1}{4}.$$

Using this value for $\overline{(e_r \cdot \mathbf{S})^2}$ and the eigenvalues of L^2, S^2, and J^2 which are $L(L+1)$, $S(S+1)$, and $J(J+1)$ respectively, (1) becomes

$$\overline{\mathbf{H}_{el}} = -\frac{2\mu_0}{r^3}\left[L(L+1) - S(S+1) + \frac{3}{4}\right]\frac{\mathbf{J}}{J(J+1)}.$$

Since we have chosen the particular case for which $S = \frac{1}{2}$,

$$\overline{\mathbf{H}_{el}} = -\frac{2\mu_0}{r^3}\left[\frac{L(L+1)}{J(J+1)}\right]\mathbf{J}.$$

The hyperfine structure interaction is then given by

$$W = \langle J| -\boldsymbol{\mu}_I \cdot \mathbf{H}_{el}|J\rangle = -2g_I\mu_N\mu_0 \left\langle \frac{1}{r^3} \right\rangle \left[\frac{L(L+1)}{J(J+1)}\right] \mathbf{I}\cdot\mathbf{J}, \qquad (8)$$

where g_I is the nuclear g-factor, $\mathbf{I}$ is the nuclear angular momentum vector, and μ_N is the nuclear magneton. $\vec{\boldsymbol{\mu}}_I = g_I\mu_N\mathbf{I}$ and $\mu_N = e\hbar/2Mc = 5.05038 \times 10^{-24}$ erg/gauss where M is the mass of the proton.

The vector model for the hydrogenlike atom (assuming Russell-Saunders coupling) is shown in Fig. 3. It will be helpful in evaluating

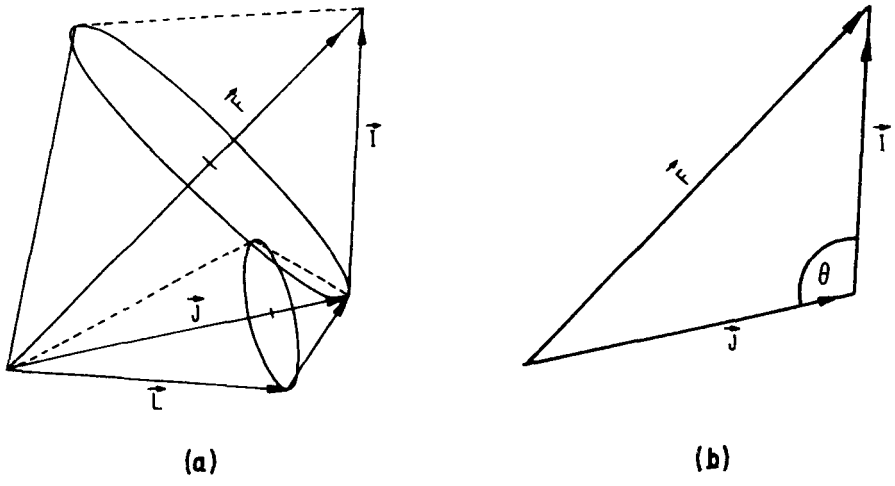

FIG. 3. Vector model for hydrogenlike atom.

$\mathbf{I}\cdot\mathbf{J}$, where $\mathbf{I}$ is the nuclear angular momentum vector, and $\mathbf{F}$ is the total angular momentum vector for the atom. $\mathbf{L}$ and $\mathbf{S}$ precess rapidly about $\mathbf{J}$ because of spin orbit interaction. $\mathbf{J}$ and $\mathbf{I}$ are magnetically coupled to a lesser degree and precess relatively slowly about $\mathbf{F}$. The angle θ of Fig. 3(b) is given by the law of cosines:

$$\cos\theta = \frac{I^2 + J^2 - F^2}{2IJ},$$

so that we may write

$$\mathbf{I}\cdot\mathbf{J} = \frac{1}{2}[I(I+1) + J(J+1) - F(F+1)].$$

Now

$$W = -g_I\mu_N\mu_0 \frac{L(L+1)}{J(J+1)}[I(I+1) + J(J+1) - F(F+1)]\left\langle \frac{1}{r^3} \right\rangle. \qquad (9)$$

The quantity $\langle(1/r^3)\rangle$ can be evaluated from the known wave functions of hydrogenlike atoms. The result is

$$\left\langle \frac{1}{r^3} \right\rangle = \frac{Z^3}{a_0^3 n^3 L(L+1)(L+\frac{1}{2})}, \tag{10}$$

where a_0 is the radius of the first Bohr orbit [$a_0 = (\hbar^2/me^2) = 5.2917 \times 10^{-9}$ cm], n is the principle quantum number, and Z is the charge on the nucleus. Finally,

$$W = \frac{g_I \mu_N \mu_0 Z^3}{a_0^3 n^3} \left[\frac{F(F+1) - I(I+1) - J(J+1)}{J(J+1)(L+\frac{1}{2})} \right]. \tag{11}$$

The various constants can be grouped and written in terms of the Rydberg and the fine structure constants, R_y and α:

$$R_y = \frac{me^4}{4\pi\hbar^3 c} \text{ (cm}^{-1}\text{)},$$

and

$$\alpha = \frac{e^2}{\hbar c}.$$

These have been determined more accurately than the result obtained for each by combining the separate constants. In terms of R_y and α

$$W = \pi\hbar c R_y \alpha^2 \left(\frac{m}{M}\right) \frac{g_I Z^3}{n^3} \left[\frac{F(F+1) - I(I+1) - J(J+1)}{J(J+1)(L+\frac{1}{2})} \right]. \tag{12}$$

Frequently, W is written as

$$W = a\mathbf{I} \cdot \mathbf{J},$$

where

$$a = \frac{2\pi\hbar c R_y \alpha^2 (m/M) g_I Z^3}{J(J+1)(L+\frac{1}{2}) n^3}.$$

It is evident from Eq. (12) that the interaction between the electron and nucleus splits a given electronic state into a number of hyperfine levels. They are designated by the various values of the total angular momentum quantum number F. The separations between the F levels fall in the radio and microwave frequency ranges of the electromagnetic spectrum. F can have the values

$$F = I + J, I + J - 1, I + J - 2, \ldots, I - J$$

if $I \geqq J$ or

$$F = J + I, J + I - 1, \ldots, J - I$$

if $J \geqq I$. The total number of possible F states is $2J + 1$ if $I \geqq J$ and $2I + 1$ if $I \leqq J$. Actually Eq. (12) is not valid for $L = 0$. In this case $\langle(1/r^3)\rangle$ vanishes (*9*). The more sophisticated relativistic caclulation yields the same result as (12) so that Eq. (12) is a valid approximation.

For hydrogen in its ground electronic state, $L = 0$, $J = \frac{1}{2}$, $g_I \approx 5.56$, and $I = \frac{1}{2}$ so that F can have only the two values, 1 and 0. Then, putting numerical values into Eq. (12), the separation between the $F = 1$ and $F = 0$ states is 1417 Mc. The experimental value obtained with atomic beam techniques is 1420.40573 $\pm$ 0.00005 Mc (*10*). More refined calculations yield almost exact agreement with experimental values for the hfs separation in hydrogen and deuterium.

The accurate calculation of the hfs separation for cesium has not been calculated nor is it likely to be in the near future. The large number of electrons, 55, for cesium makes the calculation extremely difficult. The frequency of this hfs separation in cesium is the present standard of frequency. The actual number is assigned with reference to astronomical time.

III. The Vector Model

The vector model is a simple and useful concept for the analysis of the fine and hyperfine structure of atoms in either very weak or very strong externally applied fields. For very precise measurements and for intermediate field conditions more detailed considerations are needed. These will be discussed in Section IV.

A. Weak Magnetic Fields

When the interaction between the spin and orbital motion of the electron is much greater than their interaction energy with the externally applied field, the field is considered weak. The resulting splitting that occurs is referred to as the Zeeman effect of the fine structure. Correspondingly, when the interaction energy between the nuclear moment with the electronic angular momentum is much greater than the interaction with an external field, the field is considered weak. It gives rise to the Zeeman effect of the hyperfine structure (hfs).

Consider an atom with zero nuclear spin. Under weak field conditions $\mathbf{L}$ and $\mathbf{S}$ add vectorially, and the total angular momentum is $\mathbf{J} = \mathbf{L} + \mathbf{S}$. $\mathbf{L}$ and $\mathbf{S}$ are strongly coupled and precess rapidly about $\mathbf{J}$. The vector $\mathbf{J}$, in turn, precesses slowly about the applied magnetic field $\mathbf{H}_0$. A given electronic state will be split into a number of substates. The energies of the various substates relative to the zero field energy are given by the Hamiltonian

$$\mathcal{H} = -\boldsymbol{\mu}_J \cdot \mathbf{H}_0 = g_J \mu_0 \mathbf{J} \cdot \mathbf{H}_0.$$

From the vector model (Fig. 4),

$$\mathbf{J} \cdot \mathbf{H}_0 = JH_0 \cos(\mathbf{J},\mathbf{H}_0) = m_J H_0$$

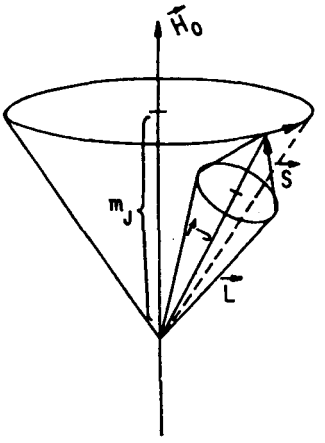

FIG. 4. Vector model of atom with zero nuclear spin.

so that

$$W = g_J \mu_0 m_J H_0, \tag{13}$$

where

$$m_J = J, J-1, \ldots, -J.$$

It is necessary to write g_J in terms of known quantities. It can be written in terms of the known g-factors of the electron, $g_S \approx 2$ and $g_L = 1$. This can be done in the following way. The projection of $\boldsymbol{\mu}_L$ and $\boldsymbol{\mu}_S$ on the direction of **J** is

$$|\boldsymbol{\mu}_J| = g_J \mu_0 J = g_L \mu_0 L \cos(\mathbf{L},\mathbf{J}) + g_S \mu_0 S \cos(\mathbf{S},\mathbf{J}).$$

Then

$$g_J = \frac{1}{J}[g_L L \cos(\mathbf{L},\mathbf{J}) + g_S S \cos(\mathbf{S},\mathbf{J})].$$

Using the law of cosines and the vector model in addition to the quantum mechanical equivalents of S^2, L^2, and J^2, we have

$$g_J = \left\{ g_L \left[\frac{J(J+1) + L(L+1) - S(S+1)}{2J(J+1)} \right] + g_S \left[\frac{J(J+1) + S(S+1) - L(L+1)}{2J(J+1)} \right] \right\}. \tag{14}$$

This expression for g_J, together with Eq. (13), gives the eigenvalues of the Hamiltonian when Russell-Saunders coupling applies. The important selection rules for transitions between sublevels of a given J and sublevels belonging to different J are $\Delta J = 0, \pm 1$ and $\Delta m_J = 0, \pm 1$.

Now suppose that the nucleus has a spin I different from zero. The vector model is shown in Fig. 3 and described in Section II page 6. **I** and **J** precess about **F**, and **F** precesses relatively slowly about the small field $\mathbf{H}_0$.

The portion of the total Hamiltonian of interest is

$$\mathcal{H} = a\mathbf{I} \cdot \mathbf{J} + g_F \mu_0 \mathbf{F} \cdot \mathbf{H}_0. \tag{15}$$

A quadrupole term is not included because we will confine ourselves to the case where $J = \frac{1}{2}$. For this case, the quadrupole term will not affect the state separations. The first term in Eq. (15) is the hfs interaction in zero field. It has been considered in Section II. The second term gives the splitting of the various possible F states in the weak field $\mathbf{H}_0$. Within the present approximation, the relative energies of the substates for a given F are

$$W_F = g_F \mu_0 m_F H_0. \tag{16}$$

The quantity g_F may be written in terms of g_J and g_I just as g_J had been previously written in terms of g_S and g_L.

From the vector model

$$g_F = \frac{1}{F} [g_J J \cos(\mathbf{J}, \mathbf{F}) - g_I I \cos(\mathbf{I}, \mathbf{F})]$$

and

$$g_F = g_J \left[\frac{F(F+1) + J(J+1) - I(I+1)}{2F(F+1)} \right] + g_I \left[\frac{F(F+1) + I(I+1) - J(J+1)}{2F(F+1)} \right]. \tag{17}$$

Equations (16) and (17) give a rather good quantitative estimate of the splitting in weak fields.

Let us consider the case when $J = \frac{1}{2}$—atoms in $^2S_{1/2}$ and $^2P_{1/2}$ states, for example. There are only two hyperfine levels—$F = I + \frac{1}{2}$ and $F = I - \frac{1}{2}$. Let these two values of F be designated by F_+ and F_-, respectively. The g-factors for these two levels are:

$$g_{F_+} = \left(\frac{1}{2I+1} \right) g_J + \left(\frac{2I}{2I+1} \right) g_I, \tag{18a}$$

and

$$g_{F_-} = -\left(\frac{1}{2I+1} \right) g_J + \left(\frac{2I+2}{2I+1} \right) g_I. \tag{18b}$$

Note that the g_F values are slightly different for the two values of F. The splitting in the two F levels in a weak field will then be slightly different. The energy level diagram may be drawn using Eqs. (16) and (18).

The diagram for cesium is shown in Fig. 5. The ground electronic state is $^2S_{1/2}$ so that $J = \frac{1}{2}$; the nuclear spin of cesium-133 is $\frac{7}{2}$. The best value

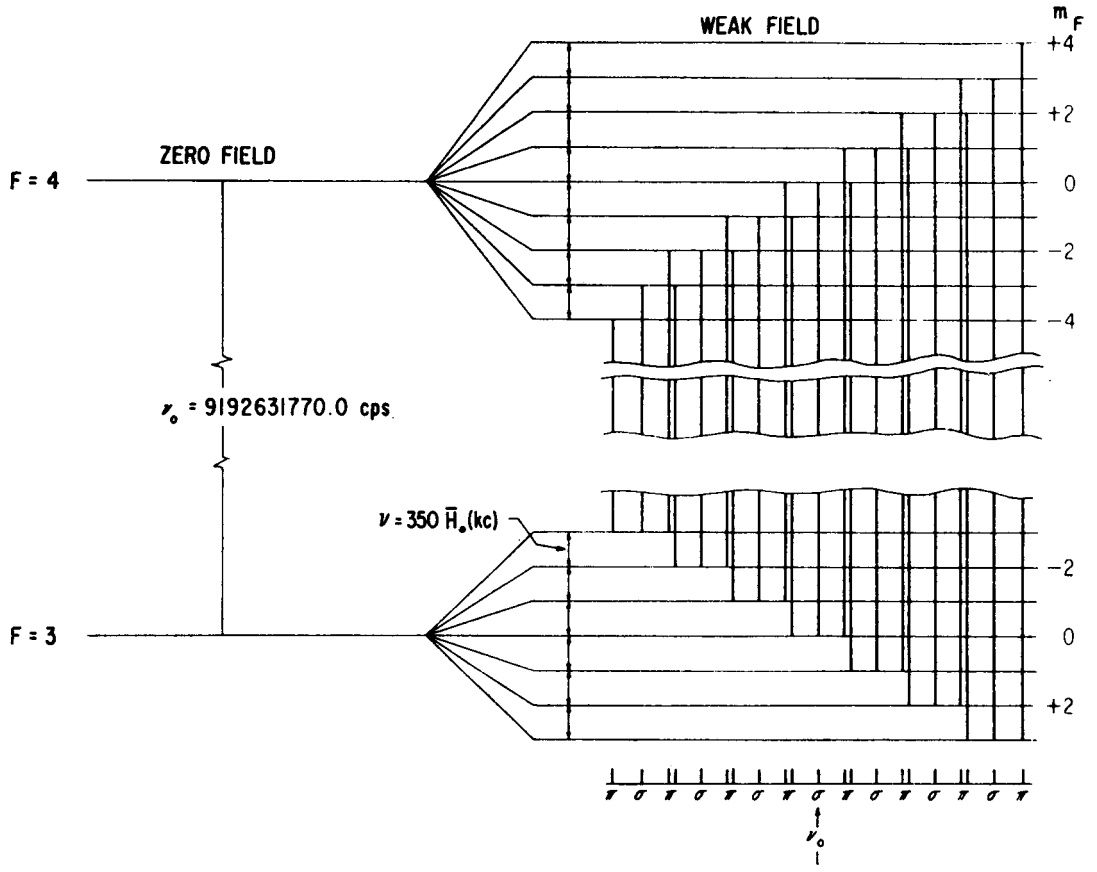

FIG. 5. Energy level diagram for Cs^{133}. The nuclear moment is positive, $I = 7/2$, and $J = 1/2$. The selection rules are $\Delta F = 0, \pm 1$; $\Delta m_F = 0, \pm 1$.

of g_I is obtained from the measured value of the magnetic moment of the cesium-133 nucleus:

$$\mu_{Cs} = +2.57887 \text{ in units of the nuclear magneton } \mu_N;$$

$$g_I = \frac{-(\text{magnetic moment in units of } \mu_N)}{(\text{angular momentum in units of } \hbar)},$$

$$g_I = -0.737.$$

In units of the Bohr magneton,

$$g_I = -0.737 \frac{m}{M} = -4.01 \times 10^{-4}.$$

Since Eq. (16) was written in terms of the Bohr magneton μ_0, these are the units of g_I that must be used.

The sequence of m_F states is inverted in the $F = 3$ level with respect to that in the $F = 4$ level as a result of the minus sign of the first term of Eq. (18b). The $F = 4$ level is higher than the $F = 3$ level. This can be seen

from the following considerations. The magnetic moment associated with the angular momentum **J** is antiparallel to **J**. The magnetic moment of the nucleus is parallel to **I** in the case of cesium (the usual circumstance). If **I** is parallel to **J**, the magnetic moments are antiparallel and the energy of interaction is evidently greater than if **I** is antiparallel to **J**. Thus when g_I is negative (and μ_I positive), the state $F = I + \frac{1}{2}$ lies above the state $F = \mathrm{I} - \frac{1}{2}$.

The closely spaced doublets appearing in Fig. 5—of which there are six—have a separation

$$\Delta\nu_{\text{doublet}} = \frac{\mu_0 H_0}{h}[2g_I] \sim 1.1 \times 10^3 \text{ sec}^{-1} \text{ gauss}^{-1},$$

which is a very small frequency separation at the field intensities normally used in atomic frequency standards (~0.010–0.100 oe). The transition $(F = 4, m_F = 0) \leftrightarrow (F = 3, m_F = 0)$ is chosen as the standard frequency transition because it is insensitive to the magnetic field. In fact, in the vector model approximation it is completely insensitive to the field. A more exact treatment shows a small quadratic field dependence of the transition frequency, as we shall see. The field sensitive lines provide a useful measure of the uniform field of the beam standard.

B. Strong Magnetic Fields

The vector model also provides a good approximation under conditions of very strong fields. The external field is said to be strong when the interaction energy between the nuclear moment and the electronic angular momentum is much less than the coupling with the field. Under these conditions **I** and **J** decouple and precess independently about the field direction (Fig. 6). The Hamiltonian is given by

$$\mathcal{H} = a\mathbf{I} \cdot \mathbf{J} + g_J\mu_0\mathbf{J} \cdot \mathbf{H}_0 + g_I\mu_N\mathbf{I} \cdot \mathbf{H}_0. \tag{19}$$

In this case the first term is not large compared with the other terms.

In the strong-field approximation $\mathbf{I} \cdot \mathbf{J}$ can be evaluated from the vector model (Fig. 6): **J** precesses much more rapidly about $\mathbf{H}_0$ than does **I**. We may then consider the average value of **J**—which is its component along $\mathbf{H}_0$—as interacting with **I**. Thus,

$$\mathbf{I} \cdot \mathbf{J} = IJ \cos(\mathbf{J}, \mathbf{H}_0) \cos(\mathbf{I}, \mathbf{H}_0),$$

and

$$\mathbf{I} \cdot \mathbf{J} = m_I m_J.$$

The energy eigenvalues are then given by

$$W = am_I m_J + g_J\mu_0 m_J H_0 + g_I\mu_N m_I H_0 \tag{20}$$

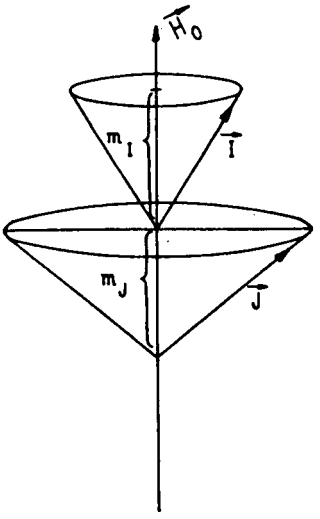

FIG. 6. Vector model of atom in strong magnetic field.

in very strong fields. This relation is a rather good approximation for cesium for fields greater than about 5000 oe.

IV. THE BREIT-RABI FORMULA (*7, 11*)

The vector model does not give an estimate of the energy separations in intermediate fields nor does it give a close enough approximation in weak and strong fields for precise beam experiments. The energy levels in any external magnetic field can be determined from the Hamiltonian:

$$\mathcal{H} = a\mathbf{I}\cdot\mathbf{J} + \mu_0 g_J \mathbf{J}\cdot\mathbf{H}_0 + \mu_0 g_I \mathbf{I}\cdot\mathbf{H}_0 + \frac{b[3(\mathbf{I}\cdot\mathbf{J})^2 + \tfrac{3}{2}\mathbf{I}\cdot\mathbf{J} - \mathbf{I}^2\mathbf{J}^2]}{2I(2I-1)J(2J-1)}. \quad (21)$$

The last term is due to the interaction between the electric quadrupole moment of the nucleus and the electronic charge distribution. There will be no quadrupole interaction in the case $J = \frac{1}{2}$ where the electronic charge distribution is spherically symmetric. This is the case that applies to existing atomic beam standards, and this is the only case that we will consider.

For $J = \frac{1}{2}$ it is necessary to diagonalize the secular determinant associated with the Hamiltonian

$$\mathcal{H} = a\mathbf{I}\cdot\mathbf{J} + \mu_0 g_J \mathbf{J}\cdot\mathbf{H}_0 + \mu_0 g_I \mathbf{I}\cdot\mathbf{H}_0.$$

The solutions are

$$W_{F=I\pm\frac{1}{2},\,m_F} = \frac{-\Delta W}{2(2I+1)} + \mu_0 g_I m_F H_0 \pm \frac{\Delta W}{2}\left[1 + \frac{4m_F x}{(2I+1)} + x^2\right]^{\frac{1}{2}}. \quad (22)$$

ΔW is the hfs separation in zero field ($\Delta W = h\nu_0$) between the states $F = I + \frac{1}{2}$ and $F = I - \frac{1}{2}$;

$$x = \frac{(g_J - g_I)\mu_0 H_0}{\Delta W}.$$

In accordance with the usual convention, the quantum numbers F and m_F are used with the understanding that at high fields these are the quantum numbers of the state from which the high field state is adiabatically derived. Equation (22) is called the Breit-Rabi formula, first given by Breit and Rabi in 1931 (*12*).

The energy level scheme is shown in Fig. 5 for weak applied magnetic fields. The transition most insensitive to the field is the $(F = 4, m_F = 0) \leftrightarrow (F = 3, m_F = 0)$ transition. The slight field dependence of the frequency of this transition is given by the Breit-Rabi formula, Eq. (22). Assuming small H_0:

$$\nu = \nu_0 + \frac{\nu_0}{2} x^2 - \frac{\nu_0}{8} x^4 + \cdots$$

Introducing the x-value for Cs^{133},

$$\nu = \nu_0 + 427.18 H_0^2 - 9.93 \times 10^{-6} H_0^4, \tag{23}$$

where ν is in cps and H_0 in oersted. The term involving H_0^4 is entirely negligible since H_0 falls in the range 0.1 to 0.01 oe for most cesium beam standards.

Equation (23) gives the zero field hfs separation ν_0 from the measured frequency ν after the value of H_0 is determined. The field H_0 can be easily evaluated by measuring any of the other observable transitions. For example, the microwave transitions ($\Delta F = \pm 1$, $\Delta m_F = 0$) for which

$$\begin{aligned} \nu_{(F=4,m_F)\leftrightarrow(F=3,m_F)} &= \nu_0 \left[1 + \frac{m}{4} x + \frac{1}{2}\left(1 - \frac{m_F^2}{16}\right) x^2 \right] \\ &= \nu_0 + 7.0062 \times 10^5 m_F H_0 + 26.699(16 - m_F^2) H_0^2. \end{aligned} \tag{24}$$

The very low frequency transitions between the sublevels of a given F state ($\Delta F = 0$, $\Delta m_F = \pm 1$) can also be used. In this case

$$\begin{aligned} \nu_{3,m_2\leftrightarrow 3,m_1} &= \frac{-\mu_0 g_I}{h} H_0 + \frac{\nu_0}{2}\left[\frac{1}{4} x - \frac{1}{32}(2m_1 - 1) x^2 \right] \\ &= 350.870 \times 10^3 H_0 - 13.349(2m_1 - 1) H_0^2, \end{aligned} \tag{25}$$

or

$$\begin{aligned} \nu_{4,m_2\leftrightarrow 4,m_1} &= \frac{\mu_0 g_I}{h} H_0 + \frac{\nu_0}{2}\left[\frac{1}{4} x - \frac{1}{32}(2m_1 + 1) x^2 \right] \\ &= 349.746 \times 10^3 H_0 - 13.349(2m_1 + 1) H_0^2. \end{aligned} \tag{26}$$

The magnetic quantum number m_1 is associated with the lower of the two substates involved in the transition. For the small values of H_0 ordinarily

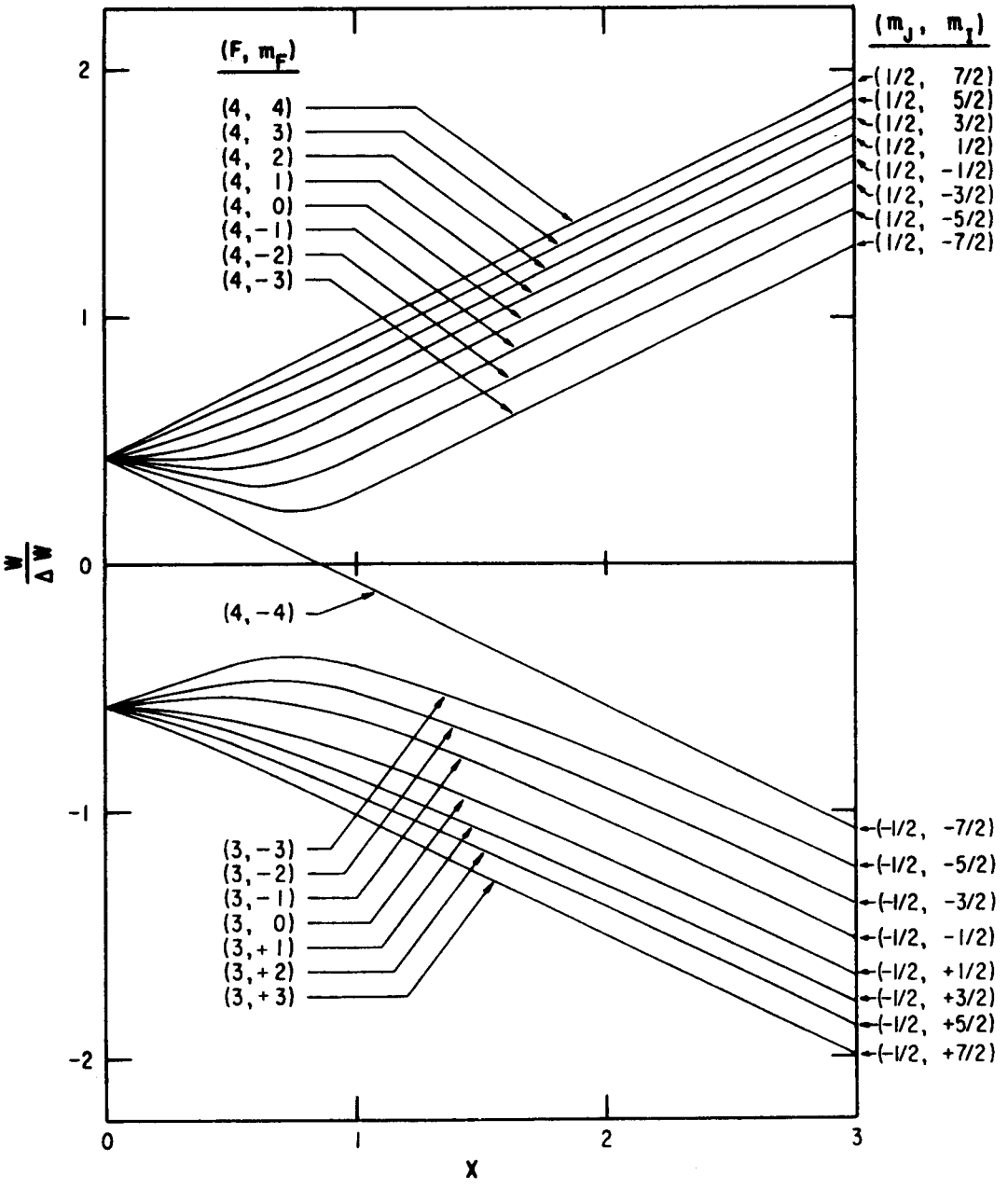

FIG. 7. Energy level diagram of Cs^{133} in the $^2S_{1/2}$ ground state as a function of the applied magnetic field. The hfs separation is $\Delta W = h\nu_0$.

used, all of the transitions of Eqs. (25) and (26) coincide at least for the practical purpose of measuring H_0.

Figure 7 shows a plot of the energy levels as H_0 varies from zero to very large values. The vector model applies in the extreme left hand and right hand sides of the graph. Equation (22) must be used for intermediate points.

V. The Atomic Beam Spectrometer

The frequencies of separation between the hfs levels in atomic spectra can be measured very precisely by means of atomic beam techniques. A schematic of a typical spectrometer used in atomic beam resonance experiments is shown in Fig. 8a, b. Many variations in design exist depending on the nature of the atom to be investigated. The design that will be discussed

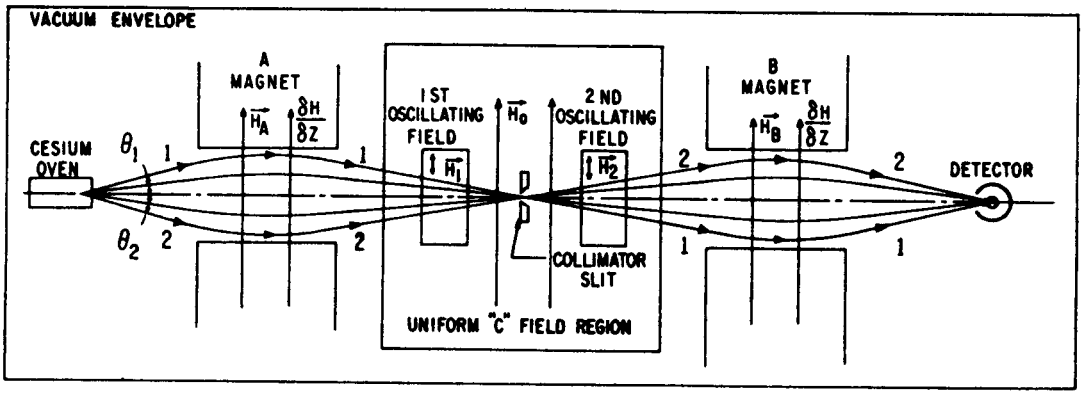

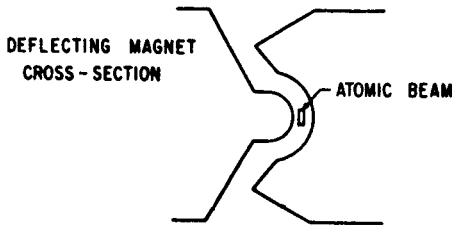

(a)

FIG. 8a. A schematic of a typical atomic beam spectrometer. The indicated trajectories are for atoms that make transitions.

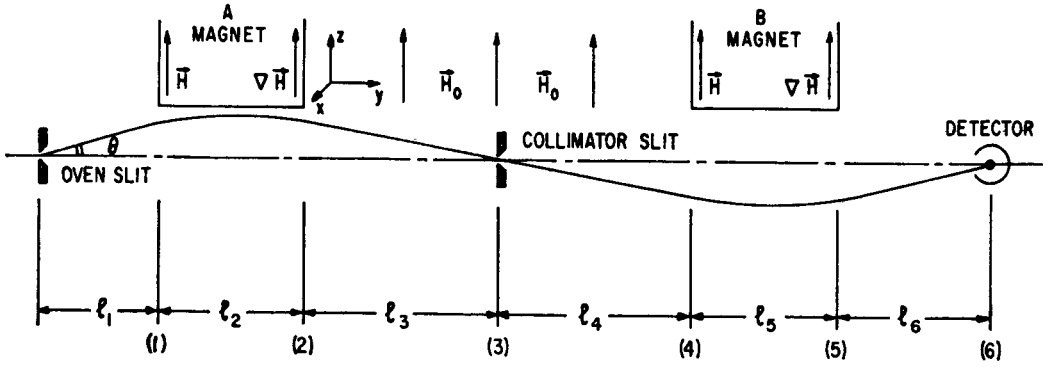

(b)

FIG. 8b. The trajectory of a single atom leaving the source at an angle θ and with a particular speed v.

here applies particularly to the longer of the two National Bureau of Standards cesium beam frequency standards (when specific numbers are given).

Neutral atoms effuse from the oven at the left in Fig. 8 and pass through the nonuniform magnetic field of the A deflecting magnet. The atoms have a magnetic dipole moment and consequently transverse forces act upon them in this nonuniform field. The magnitude and direction of this force depends upon which of the states a particular atom is in. Of all the atoms effusing from the oven at angle θ_1 and speed v suppose those in the upper group of levels of Fig. 8 (electron spin "up", or $m_J = +\frac{1}{2}$)[3] have their trajectories bent toward the axis and follow the path 1. All atoms in the lower group of levels (electron spin "down", or $m_J = -\frac{1}{2}$)[3] effusing at an angle $\theta_2 = -\theta_1$ with speed v will have their trajectories bent toward the axis also and follow a trajectory along path 2. Note that the atoms in the upper group of levels are subject to forces that are opposite in direction to the forces on atoms in the lower group—their moments have opposite sign.

The spin "up" atoms traversing the trajectory 1 and the spin "down" atoms traversing the trajectory 2 will cross the axis at the collimator slit, pass through the slit and enter the region of the B deflecting magnet. The B magnetic field is exactly like that of the A magnet. Consequently, the transverse forces of the atoms will be the same as in the A magnetic field. The spin "up" atoms will experience a downward force as before and the spin "down" atoms will experience an upward force, as before. However, now the atoms have crossed the center line at the collimator slit and the forces will tend to make the trajectories diverge from the center line. If, however, a radiation field is applied in the uniform C field region between the A and B magnets of frequency

$$\nu = \nu_0 + 427H_0^2,$$

transitions will take place between the states ($F = 4$, $m_F = 0$) and ($F = 3$, $m_F = 0$). The magnetic moments will be flipped. Atoms in the upper state will be induced to emit, and atoms in the lower state will absorb a quantum of energy—with a certain probability. Thus the sign of the magnetic moment will change for all atoms undergoing a transition. Consequently, the forces on these atoms will be opposite in the B magnet's field to what they were in the A magnet's field and they will be refocused unto the axis at the detector.

As the frequency of the exciting radiation is swept through ν, the detected signal will increase and reach a maximum at frequency ν and then decrease as the radiation frequency is varied beyond ν.

[3] It is assumed that the deflecting fields are strong fields for the purpose of qualitative discussion.

A. *Atomic Trajectories (6, 7)*

The atomic trajectories and deflections can be calculated rather simply for the elementary field configurations ordinarily used in the deflecting fields of atomic beam machines. The energy W of the atom is given by the Breit-Rabi formula, Eq. (22). This energy is a function of the magnitude of the field intensity H. The fields of the deflection magnets are conservative so that the force on the atom is given by[4]

$$\mathbf{F} = -\nabla W. \tag{27}$$

This can be rewritten as

$$\mathbf{F} = -\frac{\partial W}{\partial H}\nabla H, \tag{28}$$

provided that the only dependence of W on position is through the spatial variation of the magnetic field intensity H. $\mathbf{F}$ is different from zero only when the field has a gradient different from zero, i.e., when the field is nonuniform.

The partial derivative, $-\partial W/\partial H$, is called the effective magnetic dipole moment μ_{eff}. The effective dipole moment has, in general, a different value for each state:

$$\mu_{eff} = \mu_{F=I\pm\frac{1}{2},m_F}$$
$$= -g_I\mu_0 m_F \mp \left\{\frac{(x/2) + m_F/(2I+1)}{[1 + 4m_F/(2I+1) + x^2]^{\frac{1}{2}}}\right\}\mu_0(g_J - g_I) \tag{29}$$

for atoms with $J = \frac{1}{2}$. Note that μ_{eff} is a function of H. The magnetic moments given by Eq. (29) are plotted in Fig. 9 for cesium as a function of H (or x).

Equation (*28*) can be conveniently written as

$$\mathbf{F} = \mu_{eff}\nabla H. \tag{30}$$

The A and B deflecting magnets are designed such that the field configuration has a simple calculable form,[5] and so that the force has the components

$$F_x = 0,$$
$$F_y = 0,$$

and

$$F_z = \mu_{eff}\frac{\partial H}{\partial z} = \text{constant},$$

[4] Here $\mathbf{F}$ is the force vector and is not to be confused with the previous $\mathbf{F}$ which represented the total angular momentum vector.

[5] We consider here the field of two parallel wires with currents of equal magnitude flowing in the opposite direction. The fields themselves will be discussed more fully later.

within a reasonable approximation. Then

$$\ddot{z} = a = \frac{\mu_{eff}}{m}\frac{\partial H}{\partial z}, \tag{31}$$

where a is the acceleration imparted to the atom in the direction transverse to the axis of the spectrometer, and m is the mass of the atom. We choose the coordinate system where z is positive above the axis and negative below (Fig. 8b).

The acceleration a is different from zero only in the regions 2 and 5 where the field in nonuniform. Integration of Eq. (31) yields

$$\dot{z} = v_z = v_{zi} + a_i t \tag{32}$$

and

$$z = z_i + v_{zi}t + \tfrac{1}{2}a_i t^2, \tag{33}$$

where v_{zi} is the transverse velocity that the atom has as it enters the ith region, z_i is the z-coordinate of the particle as it enters this region, and t is the time spent in this region.

Atoms effuse from the source slit in all forward directions. Consider atoms emitted from the source with speed v and at an angle θ with respect to the center line of the machine. It is of interest to calculate the z-coordinate of these atoms at each of the y positions (1) through (6) (see Fig. 8b). The transverse velocity in region (1) is[6]

$$v_{z1} = v \sin\theta \approx v\theta$$

and the z-coordinate in plane (1) is

$$z_1 = v_{z1}t_1 = \theta l_1,$$

where $t_1 = (l_1/v)$.
The z-coordinate in plane (2) is given by

$$z_2 = z_1 + v_{z1}t_2 + \tfrac{1}{2}a_2 t_2^2,$$

where $t_2 = l_2/v$, so that

$$z_2 = (l_1 + l_2)\theta + \frac{1}{2}\frac{a_2 l_2^2}{v^2}.$$

Correspondingly,

$$z_3 = z_2 + v_{z2}t_3,$$

or

$$z_3 = (l_1 + l_2 + l_3)\theta + \frac{a_2 l_2(l_2 + 2l_3)}{2v^2};$$

$$z_4 = z_3 + v_{z2}t_4$$

[6] The angle θ will be very small for any atom that reaches the detector plane without collision. Hence $\sin\theta \approx \theta$ is a good approximation.

or

$$z_4 = (l_1 + l_2 + l + l_4)\theta + \frac{a_2 l_2}{2v^2}(l_2 + 2l_3 + 2l_4);$$

$$z_5 = z_4 + v_{z2}t_5 + \tfrac{1}{2}a_5 t_5^2$$

or

$$z_5 = (l_1 + l_2 + l_3 + l_4 + l_5)\theta + \frac{a_2 l_2}{2v^2}(l_2 + 2l_3 + 2l_4 + 2l_5) + \frac{a_5 l_5^2}{2v^2};$$

$$z_6 = z_5 + v_{z5}t_6$$

or

$$z_6 = (l_1 + l_2 + l_3 + l_4 + l_5 + l_6)\theta + \frac{a_2 l_2}{2v^2}(l_2 + 2l_3 + 2l_4 + 2l_5 + 2l_6) + \frac{a_5 l_5}{2v^2}(l_5 + 2l_6).$$

In order for an atom to pass through the collimating slit, z_3 must be zero. This imposes a condition on θ. In particular,

$$\theta = -\frac{a_2 l_2(l_2 + 2l_3)}{2v^2(l_1 + l_2 + l_3)}.$$

The displacement from the center line in the detector plane is then

$$z_6 = \frac{a_2 l_2(l_2 + 2l_1)(l_4 + l_5 + l_6)}{2v^2(l_1 + l_2 + l_3)} + \frac{a_5 l_5(l_5 + 2l_6)}{2v^2}.$$

From Fig. 9 it is evident that if a transition is induced for which $\Delta F = \pm 1$ and $\Delta m_F = 0$, the magnitude of the magnetic moment of the atom remains the same but the sign of the moment changes. Thus for this type of transition the forces would be equal but oppositely directed in regions (1) and (5) if

$$\left(\frac{\partial H}{\partial z}\right)_2 = \left(\frac{\partial H}{\partial z}\right)_5.$$

Hence a symmetrical apparatus would give a refocused beam at the detector wire. More specifically, if

$$l_1 = l_6,$$

$$l_2 = l_5,$$

$$l_3 = l_4,$$

and

$$\left(\frac{\partial H}{\partial z}\right)_2 = \left(\frac{\partial H}{\partial z}\right)_5,$$

463-560 O - 72 - 3

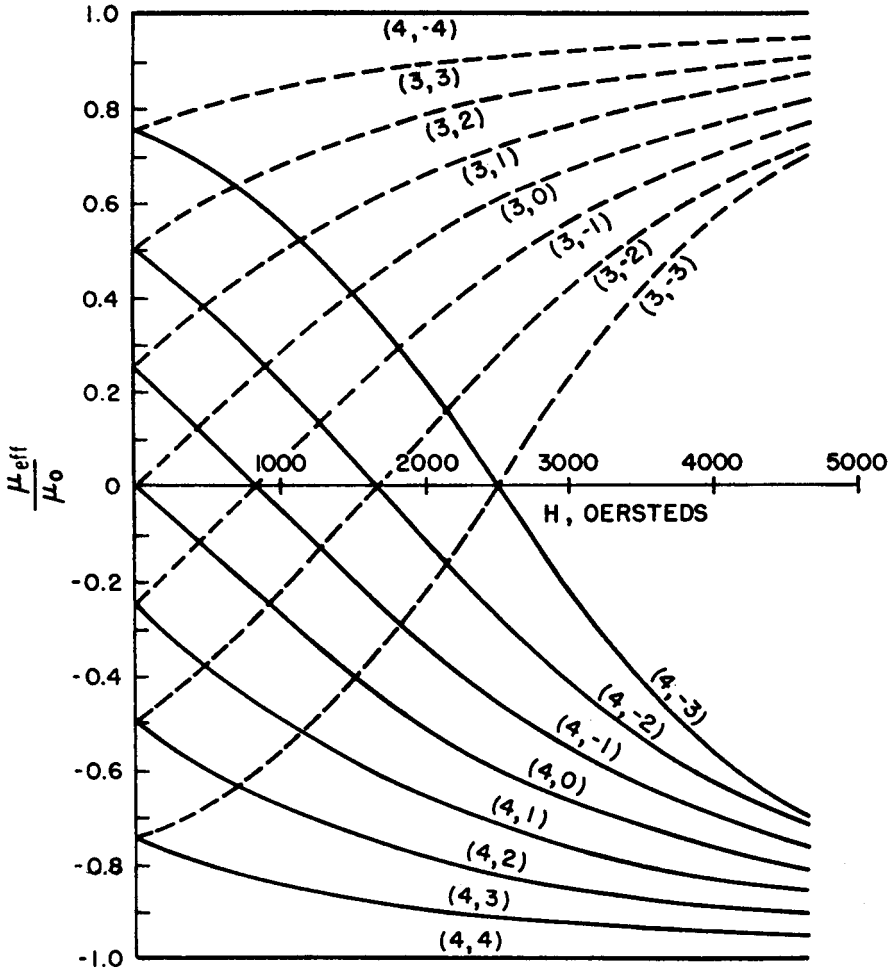

FIG. 9. The effective magnetic moment, μ_{eff}, relative to the Bohr magneton, μ_0, is plotted for the various magnetic substates in Cs^{133} as a function of the applied magnetic field.

then

$$z_6 = \frac{l_5(l_5 + 2l_6)}{2mv^2} [(\mu_{eff})_2 + (\mu_{eff})_5] \frac{\partial H}{\partial z}. \tag{34}$$

When a transition $\Delta F = \pm 1$, $\Delta m_F = 0$ is induced, $(\mu_{eff})_2 = -(\mu_{eff})_5$ and $z_6 = 0$ as described above.

Introducing some numbers, let

$$l_1 = l_6 = 24 \text{ cm},$$
$$l_2 = l_5 = 10 \text{ cm},$$
$$l_3 = l_4 = 100 \text{ cm},$$

and

$$\left(\frac{\partial H}{\partial z}\right)_2 = \left(\frac{\partial H}{\partial z}\right)_5 = 6800 \text{ oe/cm}$$

for a field at the position of the beam in the deflecting magnets of 2100 oe. For this particular value of the field intensity, $\mu_{eff} = 0.50 \times 10^{-20}$ erg/gauss. If the oven temperature is 150°C, the most probable velocity α of a cesium atom in the oven is 2.3×10^4 cm/sec and

$$z_6 = \frac{580}{4kT} [2\mu_{eff}] \frac{\partial H}{\partial z} = 0.17 \text{ cm}.$$

Although a symmetrical device is not the most suitable for observing the $\Delta F = 0$, $\Delta m_F = \pm 1$ transitions, these transitions are easily observed and they provide a useful measure of the magnitude of the uniform C field. The C field is essential in beam experiments in order to preserve the state identity of the atom as it progresses through the apparatus. All of the magnetic fields are arranged to have the same direction so that at no time will an atom in the beam pass through a region of zero field. This avoids the occurrence of nonadiabatic transitions or Majorani flop.

B. The Beam Intensity and Intensity Distribution (6, 7)

Evidently, from Eq. (34), the point at which an atom crosses the detector plane depends upon its velocity and its substate. Consider first the case when no forces are applied to the atoms of the beam, that is, when the deflecting magnets are switched off. The number of atoms striking the detector per unit time with velocities in the range v to $v + dv$ is given approximately by

$$dN = \frac{N_0 a A}{r^2} \left(\frac{m}{2\pi kT}\right)^{3/2} v^3 \exp\left(\frac{mv^2}{2kT}\right) dv. \tag{35}$$

This can be rewritten as

$$dN = I(v)dv = \frac{2I_0}{\alpha^4} v^3 \exp\left(-\frac{v^2}{\alpha^2}\right) dv, \tag{36}$$

where

$$I_0 = \frac{N_0 a A \bar{c}}{4\pi r^2} \tag{37}$$

is the total number of atoms striking the detector per unit time, N_0 is the number of atoms per unit volume in the oven, a is the oven slit area, A is the area of the detector, r is the total distance between the oven slit and the detector, $\bar{c}$ is the average speed of an atom inside the oven ($\bar{c} = \sqrt{8kT/\pi m}$), and α is the most probable speed inside the oven ($\alpha = \sqrt{2kT/m}$).

Equation (36) may be re-expressed in terms of the magnetic deflection: Let z_6 be designated as s_α when $v = \alpha$ and s otherwise so that

$$s_\alpha = \frac{2(\mu_{\text{eff}})_2}{2m\alpha^2}\left(\frac{\partial H}{\partial z}\right)_2 l_5(l_5 + 2l_6)$$

and

$$s = \frac{2(\mu_{\text{eff}})_2}{2mv^2}\left(\frac{\partial H}{\partial z}\right)_2 l_5(l_5 + 2l_6).$$

Evidently,

$$\frac{s}{s_\alpha} = \frac{\alpha^2}{v^2}$$

and

$$dN = I(s)ds = -I_0 \exp\left(-\frac{s_\alpha}{s}\right)\frac{s_\alpha^2}{s^3}\,ds \tag{38}$$

if the width of the parent beam is small compared to s.

Calculation of the actual intensity distribution must take into account the finite width of the beam. Figure 10 shows the trapezoidal beam shape

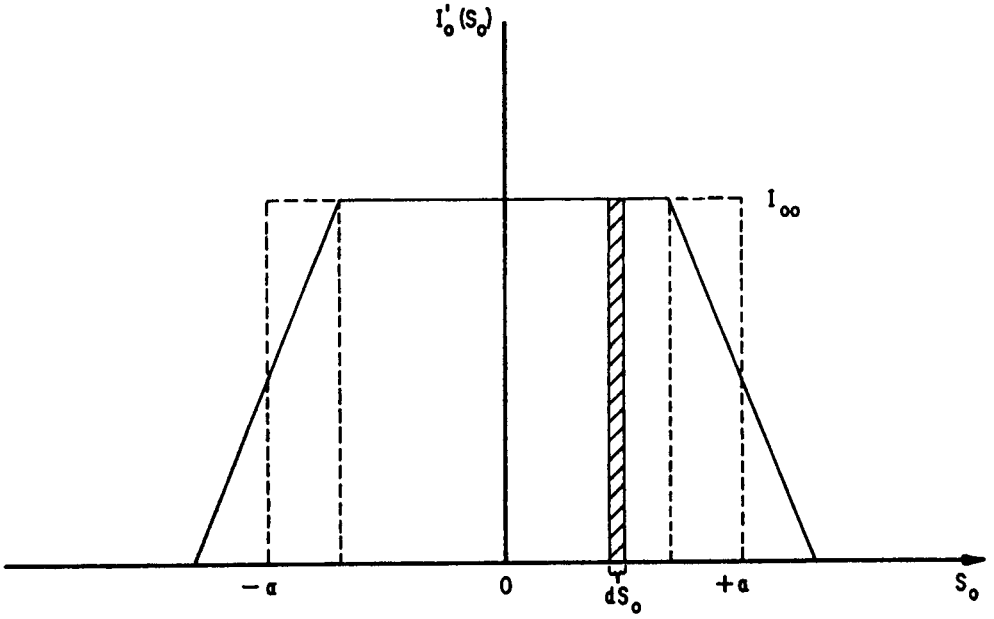

FIG. 10. Beam profile without deflection at the detector plane.

at the detector plane without deflection. The refocused beam would have the same shape if only atoms undergoing a moment change in the radiation field were considered.

Considering the finite width of the beam, the magnetic deflection is $s - s_0$ and

$$\frac{v^2}{\alpha^2} = \frac{s_\alpha}{s - s_0}.$$

Then the contribution to the intensity at s due to the infinitesimal width ds_0 at s_0 of the parent beam is given by

$$dI(s) = I_0'(s_0) \frac{s_\alpha^2}{(s - s_0)^3} \exp\left(-\frac{s_\alpha}{s - s_0}\right) ds_0, \tag{39}$$

where $I_0'(s_0)$ is the total number of atoms incident per second on the detector per unit width at the point s_0. If w is the width of the detector,

$$\int_{-w/2}^{+w/2} I_0'(s_0) ds_0 = I_0, \text{ approximately,}$$

where I_0 is given by Eq. (37).

In Eq. (39), $s - s_0$ must always have the same sign as s_α. When $s - s_0$ has the opposite sign from s_α there is no contribution at s and $dI(s) = 0$. Rather than introduce the trapezoidal shape of the undeflected beam into Eq. (39), it is usually sufficient to consider the equivalent rectangular beam shape of width $2a$ (Fig. 10). Integration of Eq. (39) yields

$$I(s) = I_{00}\left[\exp\left(-\frac{s_\alpha}{s+a}\right)\left(1 + \frac{s_\alpha}{s+a}\right) - \exp\left(-\frac{s_\alpha}{s-a}\right)\left(1 + \frac{s_\alpha}{s-a}\right)\right] \tag{40a}$$

for $s \geqq a$,

$$I(s) = I_{00}\left[\exp\left(-\frac{s_\alpha}{s+a}\right)\left(1 + \frac{s_\alpha}{s+a}\right)\right] \tag{40b}$$

for $-a \leqq s \leqq a$, and

$$I(s) = 0 \tag{40c}$$

for $s \leqq -a$. These equations apply when s_α is positive. The intensity distribution is (ideally) symmetrical about $s = 0$.

Figure 11 shows the intensity distribution for various values of s_α. It is evident from the curves that the maximum intensity occurs at a point considerably less than s_α. The probability of an atom emerging from the source slit is proportional to the velocity. Consequently, the most probable velocity in the beam is somewhat greater than the most probable velocity in the oven. In fact, the most probable velocity in the beam is $\sqrt{3/2}\alpha = 1.22\alpha$. The deflection of atoms in the beam will generally be less than s_α. The values of $|s|$ at the maxima of the curves occur at about $|s_\alpha|/3$ for large s_α ($s_\alpha \sim 10a$ or greater).

In the case of cesium, the beam is composed of atoms in 16 different states. A different μ_{eff} and s_α is associated with each state. The observed intensity distribution is then the composite of all of these separate intensity distributions. All of the separate distributions have approximately equal

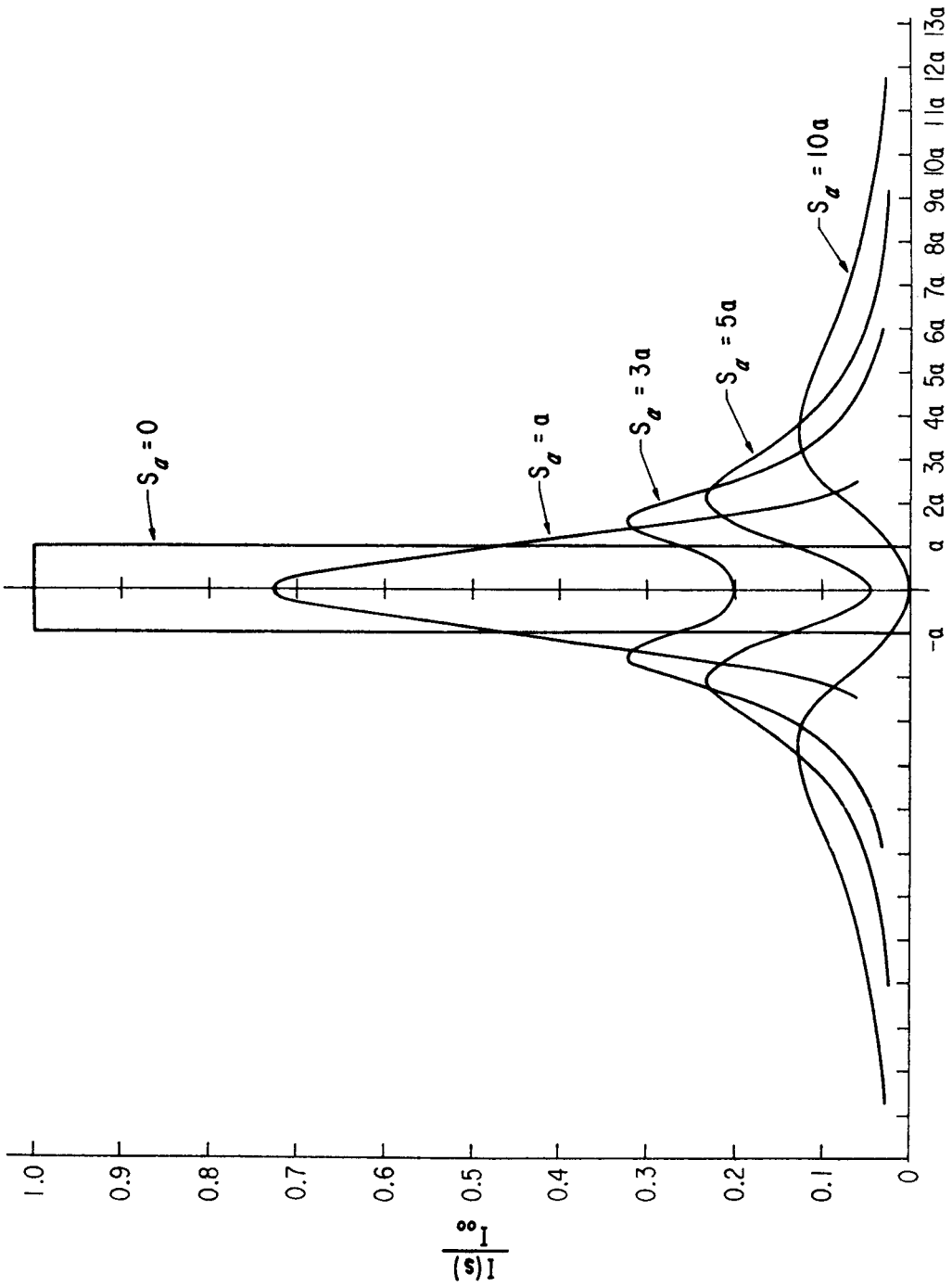

FIG. 11. The intensity distribution of the deflected beam for various values of s_a.

weight. The total intensity distribution is experimentally plotted by simply moving the detector transversely across the beam. This is a useful procedure in aligning the instrument. A suitable Stern-Gerlach peak separation is about 3 undeflected beam widths or $6a$ for a good signal-to-noise ratio of the refocused atoms. The deflecting magnets must be designed so that they are capable of providing an intensity distribution of this general character.

The observed signal in a beam experiment is the change in detector current due to the induced transitions. The total undeflected beam intensity seen by the detector centered at $s = 0$ is

$$I_0 = 16 I_{00} w, \qquad \text{if } w < 2a$$

and

$$I_0 = 16 I_{00} 2a \qquad \text{if } w > 2a,$$

where w is the width of the detector and I_{00} is the number of atoms of a single state colliding with the detector per second per unit width of detector.

Equation (37) gives a relation for I_0 if it is assumed that simple effusion occurs from the oven slit. At an oven temperature of 150°C the vapor pressure of cesium is about 5×10^{-3} mm Hg, and $N_0 \sim 1 \times 10^{14}$ atoms/cm^3. If the oven slit and detector widths are 0.015 in. and the equivalent beam height is 0.05 in., then

$$I_0 = \frac{N_0 a A \bar{c}}{4\pi r^2} \approx 8 \times 10^7 \text{ atoms/sec}$$

for $r = 268$ cm. For a surface ionization detector, the efficiency of ionization can be nearly 100%. In this case the detected current would be

$$(8 \times 10^7 \text{ electrons/sec})(1.6 \times 10^{-19} \text{ coul/electron}) = 1.3 \times 10^{-11} \text{ amp.}$$

Approximately one-eighth of this total detected intensity is contributed by the two states $(F = 4, m_F = 0)$ and $(F = 3, m_F = 0)$. When the deflection magnets are switched on, the intensity seen by the detector is

$$I' = \int_{-w/2}^{+w/2} I(s) ds.$$

If $w = a$, the integration yields

$$I' = \frac{a}{2} I_{00} [3 \exp(-2s_\alpha/3a - \exp(-2s_\alpha/a)]. \tag{41}$$

The total intensity is obtained by superposing the contributions made by all of the states, each state having in general a different s_α.

$$I'_{\text{total}} = \sum_{i=1}^{16} \eta_i I_{00} \frac{a}{2} [3 \exp(-2s_{\alpha i}/3a) - \exp(-2s_{\alpha i}/a)]. \tag{42}$$

η_i is the relative population of atoms in the ith state. If the transitions $(F = 4, m_F = 0) \leftrightarrow (F = 3, m_F = 0)$ are induced (with probability one), then the total detected intensity would be

$$I'_{\text{total}} = 2I_{00}a + \sum_{i=1}^{14} \frac{a}{2} I_{00} [3 \exp(-2s_{\alpha i}/3a) - \exp(-2s_{\alpha i}/a)], \quad (43)$$

where it is assumed that all states have equal populations. The first term is due to the refocused atoms. If the deflecting fields are very strong, then the $s_{\alpha i}$ are very nearly the same for all the states.

In order to observe the maximum change in detector signal when a transition occurs, the summation term of Eq. (43) should be made small relative to the term $2I_{00}a$ (see Fig. 11). A satisfactory practical choice of machine parameters to attain this condition are those for which $s_\alpha \approx 10a$.

Estimates of intensity by means of the foregoing relationships assume that simple effusion occurs at the oven slit and that the velocity distribution is not affected by the geometry of the apparatus. The oven slits are frequently made up of many long channels from which simple effusion does

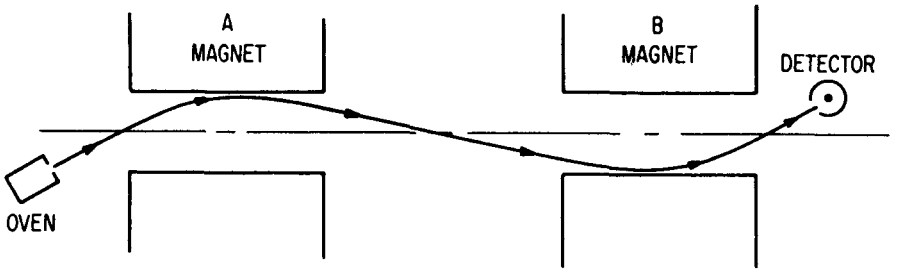

FIG. 12. Oven and detector offset arrangement for the selection of slower atoms. A narrower spectral line results.

not occur (*7*, *12*). This tends to concentrate the atoms effusing from the source within a smaller solid angle with a saving of oven material, in this case, cesium. The channeled source also tends to reduce the number of slow atoms detected because of this concentration of the beam—at least if the oven and detector are placed on the axis of the machine in the usual way.

The geometry of the apparatus will affect the velocity distribution. If the deflecting magnet pole shoes are too close together, the slow atoms that could be detected will be eliminated from the beam and the spectral line will be broad. It is useful to introduce a stop at the center of the undeflected beam for the purpose of eliminating very fast atoms. A reduction in intensity is incurred but the spectral line width will be narrower. It is thus useful to restrict the fast atoms but not the slow atoms.

Some economy in magnet construction can be gained by using deflecting magnets with rather narrow spacing between the pole shoes and off-

setting the oven and detector from the machine axis. Although the slowest atoms will be eliminated from the beam if the oven and detector are both on the machine axis, the slow atoms can be observed, together with the consequent narrower line, by offsetting the oven slit and detector (see Fig. 12). In this arrangement only emission or absorption is observed instead of both as in the usual circumstance.

C. The Deflecting Fields (6, 7)

Most atomic beam spectrometers employ iron magnets designed to produce the same field as two parallel wires carrying current in opposite directions. In a few cases, four- and six-wire field configurations have been used. The more common two-wire field will be considered first. Figure 13a

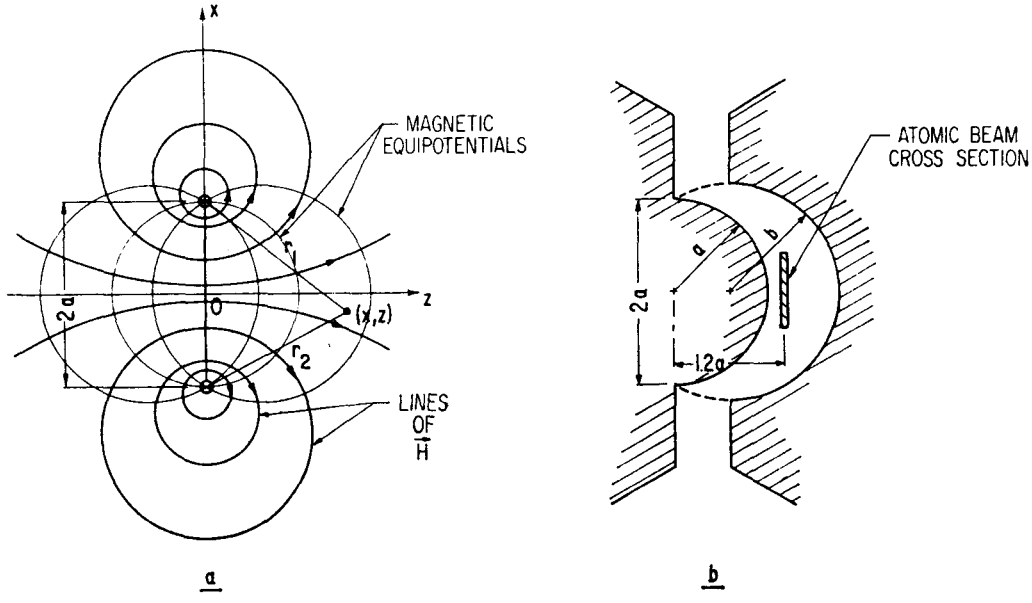

FIG. 13. (a) The field intensity lines and magnetic equipotentials of two parallel wires normal to the diagram at $x = a, z = 0$ and $x = -a, z = 0$. (b) An iron deflecting field contoured to produce a two-wire field.

displays the field intensity and the equipotentials of two parallel wires normal to the diagram at $(x = a, z = 0)$ and $(x = -a, z = 0)$. They carry a current I in opposite directions. The field intensity at the point (x, z) is given by[7]

$$H(x, z) = \frac{4Ia}{r_1 \cdot r_2} \tag{44}$$

and the gradient of the field is given by (see Appendix F in Ramsey, 7)

$$\frac{\partial H}{\partial z} = -4Ia\left(\frac{r_1^2 + r_2^2}{r_1^3 r_2^3}\right) z. \tag{45}$$

[7] In this relationship, I is measured in abamperes (1 abamp = 10 amp).

The value of this derivative $\partial H/\partial z$ is almost constant in the region $x = 0$, $z = 1.2a$. If the undeflected beam is centered at $z = 1.2a$ and the beam height does not exceed $1.4a$, the beam will be deflected without excessive distortion. It may be assumed in calculating atomic trajectories that $\partial H/\partial z$ and H both are constant in an adequately large region about this point.

At the point $y = 0$, $z = 1.2a$,

$$H = \frac{1.64I}{a},$$

$$\frac{\partial H}{\partial z} = \frac{1.61I}{a^2},$$

and

$$\frac{1}{H}\frac{\partial H}{\partial z} \approx \frac{1}{a}. \tag{46}$$

The current has been conveniently eliminated in this relationship.

The lines of **H** and the magnetic equipotentials form a system of orthogonal circles for two parallel wires. This same field configuration can be produced by an iron magnet by simply contouring the pole surfaces to coincide with two equipotential surfaces (see Fig. 13b). Suitably large deflections for cesium atoms can be obtained with rather simple low power magnets of this kind. In molecular beam experiments the effective magnetic moments of the molecules are ordinarily the order of a nuclear magneton; very large magnets are required and beam widths must be smaller. There appear to be some distinct advantages in using multipole deflecting fields. Multipole field configurations have been used successfully in atomic beam experiments (*13*, *14*, *15*) and in gaseous masers (*16*). A significant increase in intensity is gained—perhaps an order of magnitude—because these field configurations accept atoms from a relatively large solid angle. In atomic resonance beam experiments, however, a fraction of this gain is lost because of nonadiabatic transitions occurring as the beam enters and leaves the uniform C field region.

Figure 14 shows a cross section of a four-pole deflecting field. The surfaces of the iron pole pieces have been contoured to fall on the magnetic equipotentials whose intersection with the plane of the diagram form hyperbolas. The magnitude of the field intensity can be shown to be (ideally)

$$H = \frac{H_m}{R} r. \tag{47}$$

The transverse force on an atom within this magnet assembly is radial:

$$\mathbf{F} = -\nabla W = \left(-\frac{\partial W}{\partial H}\right)\frac{\partial H}{\partial r}\,\mathbf{e}_r, \tag{48}$$

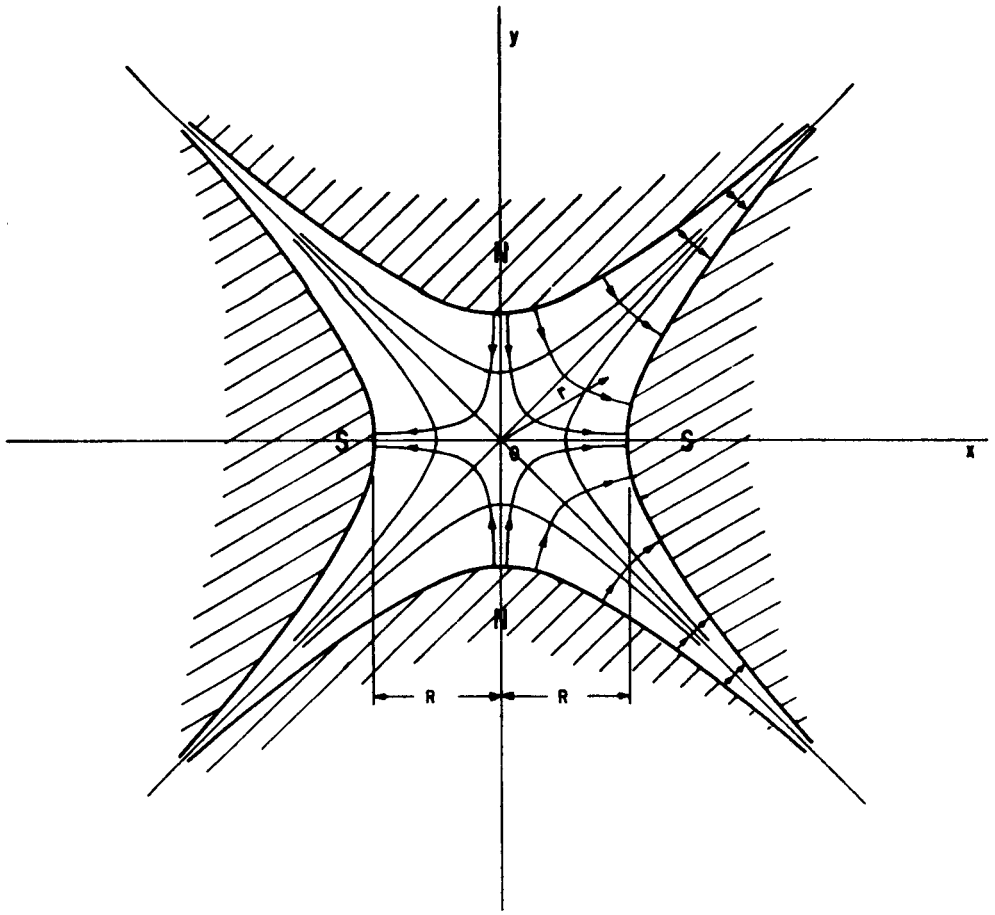

FIG. 14. Cross section of a four pole magnetic deflection field.

where $\mathbf{e}_r$ is a radial unit vector and

$$\frac{\partial H}{\partial r} = \frac{H_m}{R}. \tag{49}$$

R is the distance from the axis of the assembly to the nearest point on each of the four-pole surfaces, and H_m is the magnetic field at these points on the surfaces.

In general, W is a function of the magnitude of the field H and is given by the Breit-Rabi formula. If the field produced by the magnet assembly is sufficiently strong so that the magnetic interaction energy with the external field is large compared to the interaction energy between the nuclear and electronic angular momentum (Paschen-Back effect), then the atom will have a magnetic moment μ_{eff} of the order of a Bohr magneton independent of the magnetic field. As an example consider cesium: In strong fields

$$\mu_{eff} = -\mu_0 \text{ for } m_J = +\frac{1}{2} \text{ states}$$

and

$$\mu_{eff} = +\mu_0 \text{ for } m_J = -\frac{1}{2} \text{ states.}$$

Then

$$F_r = \mu_{eff} \frac{H_m}{R} = \mp \mu_0 \frac{H_m}{R} = \text{constant.} \tag{50}$$

Atoms for which μ_{eff} is positive are repelled from the axis, and atoms for which μ_{eff} is negative are attracted toward the axis. For atoms entering the deflecting field with a velocity vector in a plane containing the axis, the equations of motion have the same form as those previously calculated for a two-wire field. In general the atoms will execute a spiral motion through the deflecting field.

In order to consider μ_{eff} sufficiently independent of the field it would be necessary to adjust H_m to about 5 kgauss or higher for cesium and in addition a stop would be necessary on the axis so that atoms passing through the low field regions in the neighborhood of the axis would be eliminated from the beam. The stop would insure the validity of Eq. (50) which assumes μ_{eff} = constant. The field could also be operated at lower intensities in which case the force on an atom is approximately proportional to r, its distance from the axis. Cesium atoms in states ($F = 4$, $m_F = 0$) and ($F = 3$, $m_F = 0$), for example, in applied fields of 2 kgauss or less have an effective dipole moment approximately given by

$$\mu_{eff} = -\frac{\partial W}{\partial H_0} = \mp \frac{1}{2} \frac{[(g_J - g_I)\mu_0]^2}{\Delta W} H_0,$$

where the minus sign applies to the $F = 4$ state and the plus sign refers to the $F = 3$ state. The force on these atoms is

$$F_r = \mp \frac{1}{2} \frac{[(g_J - g_I)\mu_0]^2}{\Delta W} \left(\frac{H_m}{R}\right)^2 r = \mp kr, \tag{51}$$

where

$$k = \frac{1}{2} \frac{[(g_J - g_I)\mu_0]^2}{\Delta W} \left(\frac{H_m}{R}\right)^2. \tag{52}$$

Atoms in the ($F = 4$, $m_F = 0$) state are attracted toward the axis, and atoms in the ($F = 3$, $m_F = 0$) state are repelled from the axis. Atoms in the upper state would execute simple harmonic motion in passing through the deflecting field with angular frequency

$$\omega = \sqrt{\frac{k}{m}} = \mu_0 \frac{(g_J - g_I)}{(2m\Delta W)^{1/2}} \frac{H_m}{R} \tag{53}$$

A six-pole magnet with strong fields would also exert a force on the atoms proportional to r. Then

$$F_r = \mp \left(3\mu_0 \frac{H_m}{R^2}\right) r, \tag{54}$$

and

$$\omega = \sqrt{\frac{3\mu_0 H_m}{mR^2}}. \tag{55}$$

A beam device might be designed such that somewhat less than ¼ or ½ of a period of this harmonic motion occurred within each of the deflecting fields (see Fig. 15). Only flop-out experiments can be performed with these field configurations if the detector is placed on the axis as in Fig. 15a, b.

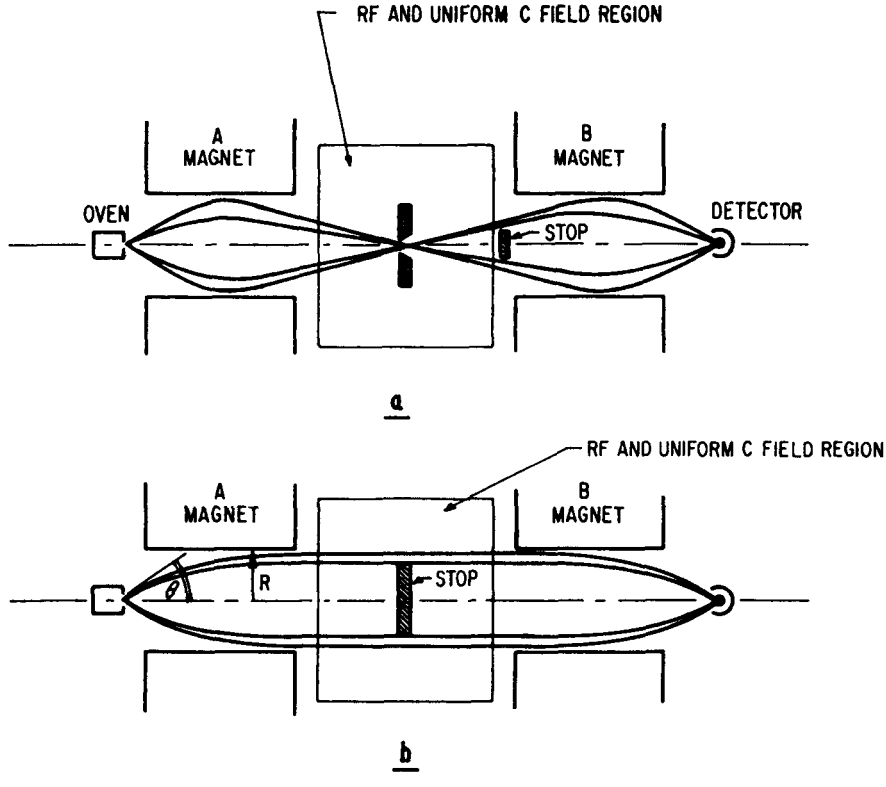

FIG. 15. (a) A beam device designed for ¼ the period of the harmonic motion occurring in the deflection magnet's field. (b) A beam device designed for ½ the period of the harmonic motion occurring in the deflection magnet's field.

The solid angle accepted from the source by the deflection magnet assembly can be determined in the following way. The increase in potential energy of an atom as it passes through the deflection field must be equal to the decrease in transverse kinetic energy that the atom experiences in passing through this field. Thus,

$$\frac{1}{2}m[v_{tr}(0)]^2 - \frac{1}{2}m[v_{tr}(R)]^2 = W(R) - W(0),$$

where $v_{tr}(0)$ is the transverse velocity of the atom as it enters the field (we assume that the oven orifice is on the axis at $r = 0$), $v_{tr}(R)$ is the transverse velocity at a distance R from the axis, and $W(R)$ and $W(0)$ are the potential energies of the atom at distances $r = R$ and $r = 0$ respectively. R is the radius of a circle inscribed within the pole pieces and touching the pole tips. For the fields considered $W(0) = 0$ and $W(R)$ are given by the Breit-Rabi formula. Presumably, only those atoms having $v_{tr}(R) \leqq 0$ will remain in the beam. An atom effusing from the source with velocity v can be emitted at a maximum angle θ_v and still remain in the beam. This angle will be sufficiently small so that we may write

$$v_{tr} = v \sin \theta_v \approx v\theta_v.$$

Now

$$\frac{1}{2}m[v_{tr}(0)]^2 = W(R) = \frac{1}{2}m[v\theta_v]^2,$$

or

$$\frac{1}{2}m[v\theta_v]^2 = \frac{kR^2}{2}.$$

The maximum solid angle accepted from the source is then

$$\Omega_v = \pi\theta_v^2 = \frac{\pi kR^2}{mv^2} \tag{56}$$

for atoms in the state considered and having velocity no less than v.

D. Beam Detection and Beam Sources (6, 7, 13, 17)

When an atom approaches a metal surface ionization processes are often possible. An atom will be ionized if an atomic electron tunnels to any unoccupied electronic state in the metal. This process occurs with particular ease for cesium. The atoms of the beam strike a hot wire, the ions are boiled off, collected, and measured with an electrometer or electron multiplier circuit. In Fig. 16 the metal is represented by a potential well of depth W_a filled with electrons to the Fermi level ζ. The work function ϕ is the minimum energy required to raise an electron to the energy continuum. The atom is represented by a second potential well which is occupied by an electron in one of the possible energy states. The ionization potential of the atom is denoted by V_I.

In order for ionization to take place, the energy level of the electron in the atom must coincide within narrow limits of a vacant energy level in the metal. The two states are then said to be in resonance and tunneling

may occur. The shapes of the potential wells of the metal and atom are deformed at close approach. This deformation is necessarily accompanied by a shift of the energy levels and consequently a shift in the ionization potential. Evidently, if an atom whose ionization potential is less than the work function of a metal strikes the metal surface, it can be re-evaporated as a positive ion (*18*). The metal must be sufficiently hot to prevent conden-

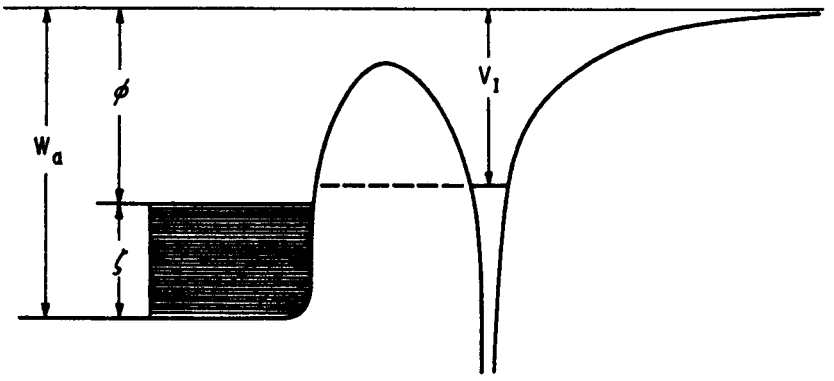

FIG. 16. A pictorial representation of the potential barrier between an atom and a metal surface.

sation. Cesium has a particularly low ionization potential (VI = 3.87 ev) and can be ionized with almost 100% efficiency on hot tungsten (ϕ = 4.5 ev) or hot platinum (ϕ = 5.1). The NBS standards employ a platinum-iridium alloy (80% Pt; 20% Ir) with somewhat improved behavior over either tungsten or platinum. There seem to be fewer impurity ions in the alloy than in tungsten. These ions create an undesirable and erratic background current.

The tungsten or Pt-Ir detector is usually in the form of a ribbon. Cesium is detected with good efficiency if the temperature of the ribbon is maintained at about 900°C. The ion current can be measured either with an electrometer or electron multiplier circuit. If an electrometer is used the ribbon is frequently surrounded by a collector ring, and if an electron multiplier is used, accelerating and focusing electrodes must be introduced. Frequently a mass spectrometer is used to analyze the ion beam, thus removing the impurity ions. The National Company Atomichron employs a tungsten ribbon together with an electron multiplier and mass spectrometer.

Electrometer circuits are capable of measuring currents as low as 1×10^{-17} amp. Those employed in the NBS standards have a background current of 4×10^{-15} amp when operating under ideal conditions. With the exciting radiation adjusted in frequency to the resonance peak of the atomic transition, the detected current is typically the order of 4×10^{-12} amp so that the signal-to-noise ratio is about 1000. Strictly speaking, this is the signal-to-noise ratio for Rabi excitation (see Section V,E). Most atomic

frequency standards employ Ramsey type excitation. The signal-to-noise ratio in this case is usually given by the ratio of the peak intensity less the intensity at the first minimum of the Ramsey interference pattern divided by the root-mean-square of the noise current. Because of the distribution of velocities in the beam, the first minimum does not go down to the noise level. In fact, typically, the current at this point is about $\frac{3}{4}$ or $\frac{2}{3}$ of the current at the peak of the spectral line. Thus the signal-to-noise ratio of the Ramsey line is about 330.

It is of interest to compare the electrometer and electron multiplier detectors. The electrometer circuit has the advantage of simplicity but the disadvantage of a longer time constant ($\sim$0.2 sec for typical current values).

A simplified model of an electrometer circuit is shown in Fig. 17. Let

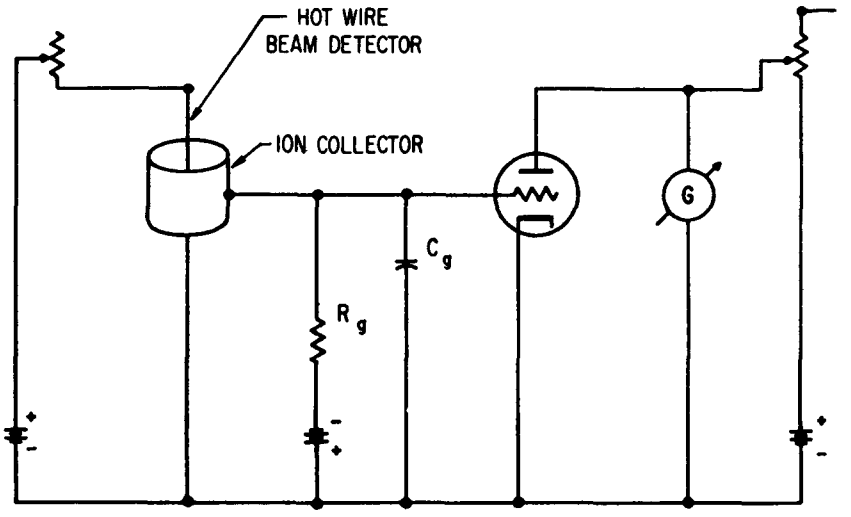

FIG. 17. Simplified electrometer circuit for the detection of atomic beam ion currents

us consider the noise in such a circuit. We will neglect the noise resulting from beam fluctuations and impurity ions boiled off the detector wire. The important sources of noise remaining are the Brownian motion of electricity in the grid circuit and the shot noise of the grid current. Using the Schottky and Nyquist relations, it can be shown (*19*, *20*) that the mean squared deviation of the grid current is given by

$$\overline{\Delta I^2} = \frac{(2kT/R_g) + eI}{2R_gC_g} \tag{57}$$

so long as the time constant τ of the galvanometer is much less than the time constant, R_gC_g, of the grid circuit. In Eq. (57), k is the Boltzman constant ($k = 1.38 \times 10^{-23}$ joules/°K), T is the absolute temperature of the grid resistor R_g, e is the electronic charge ($e = 1.60 \times 10^{-19}$ coul), and I is the grid current in amperes.

If the galvanometer responds much more slowly than the grid circuit, i.e., if $\tau \gg R_g C_g$, and if $(2kT/R_g) \gg eI$, then

$$\overline{\Delta I^2} = \frac{\pi kT}{\tau R_g}. \tag{58}$$

As an example suppose that $C_g = 20\mu\mu f$, $T = 300°K$, $R_g = 10^{10}$ ohms, and $I = 1 \times 10^{-12}$ amp. Using Eq. (57) and associated assumptions, the root-mean-square current deviation is

$$\Delta I_{rms} = 1.6 \times 10^{-15} \text{ amp.}$$

The signal-to-noise ratio is $I/\Delta I_{rms} = 630$. If the ionized beam current is measured with an electron multiplier, the primary contribution to the noise, ignoring the beam fluctuations and impurity ions, is shot-noise.

The mean squared deviation of the output noise current is given approximately by (*21*, *22*)

$$\overline{\Delta I_n^2} = 2eIM\left(\frac{mM-1}{m-1}\right)\Delta\nu, \tag{59}$$

where I is the average ion current incident on the first dynode, M is the total current multiplication factor, m is the average multiplication per stage, e is the charge on the electron, and $\Delta\nu$ is the bandwidth. It has been assumed in Eq. (59) that the probability of production of secondary electrons is given by a Poisson distribution which is only an approximately valid assumption (see *21*).

If $M = 10^6$, $m = 3$, $\Delta\nu = 5$ cps, and $I \times 10^{-12}$ amp, then the root-mean-square deviation of the output current is

$$\Delta I_{rms} = 1.5 \times 10^{-9} \text{ amp,}$$

and the signal-to-noise ratio is

$$\frac{MI}{\Delta I_{rms}} = 670,$$

which is not much different from the value obtained for the electrometer with the same time constant. This signal-to-noise ratio calculated for the electron multiplier would have to be reduced because the efficiency with which Cs^+ ions produce electrons at the first dynode is perhaps only 15% of the efficiency of an electron producing secondary electrons at this surface. Thus the estimated signal-to-noise ratio is about 100, and the electrometer appears to have some advantage over the electron multiplier. The real advantage of the electron multiplier seems to be for measuring very small currents as evidenced by Eqs. (58) and (59). Also, the time constant of the electrometer circuit becomes excessively long for very small currents.

463-560 O - 72 - 4

Various kinds of modulation schemes have come into use and are applicable to atomic beam frequency standards (*23, 24, 25*). Vibrating reed electrometers are used in both the United Kingdom and the United States frequency standards. They have some useful advantages over the dc electrometer (*26*).

The response time of electrometer circuits can be made sufficiently short for permissible modulation frequencies. (The modulation frequency must be less than the spectral line width.) By following the electron multiplier or electrometer with an amplifier and phase detector tuned to the modulation frequency, a correction signal may be obtained. This correction signal can then be used to lock the crystal oscillator from which the beam excitation is derived. Thus a signal source continuously locked to the atomic resonance is obtained. The National Company Atomichron employs this scheme of locking an oscillator to the cesium resonance (*27*).

The experience at NBS with servo devices is that manual measurements still provide the best, most consistent measurements. The feedback circuits sometimes introduce troublesome systematic errors. Even though precision and stability are good, there remains some uncertainty in accuracy. Considerable progress is being made in the improvement of the servo systems, however.

In the above considerations of noise in electrometer circuits and electron multipliers, the sources of noise originating from beam fluctuations and impurity ions boiled off of the hot wire were neglected. The noise from these sources may easily exceed those already discussed if proper care is not taken. The vacuum and beam excitation must be stable and the cesium in the source reasonably pure.

Distilled cesium of adequate purity may be obtained commercially in sealed glass ampoules. Cesium reacts with air and it is best but not necessary to break the ampoule in the oven under vacuum. The oven may also be filled with an inert gas after which the ampoule is broken and the oven immediately installed in the spectrometer. The vapor pressure of cesium as a function of temperature is shown in Fig. 18. Different groups operate the source at different temperatures ranging from about 70°C to 150°C. The source temperature depends upon the design of the oven slit and somewhat on the pumping speed. The NBS ovens are operated at 150°C at which temperature the vapor pressure of cesium is about 5×10^{-3} mm Hg. The mean free path for cesium at this pressure and temperature is approximately 5 cm. The oven slits may be channeled if it is desired to conserve cesium but they need not be unless the slit dimensions become comparable to the mean free path.

In the NBS devices, when operated with the oven slit and detector on the machine axis, it is found that the spectral line width is significantly

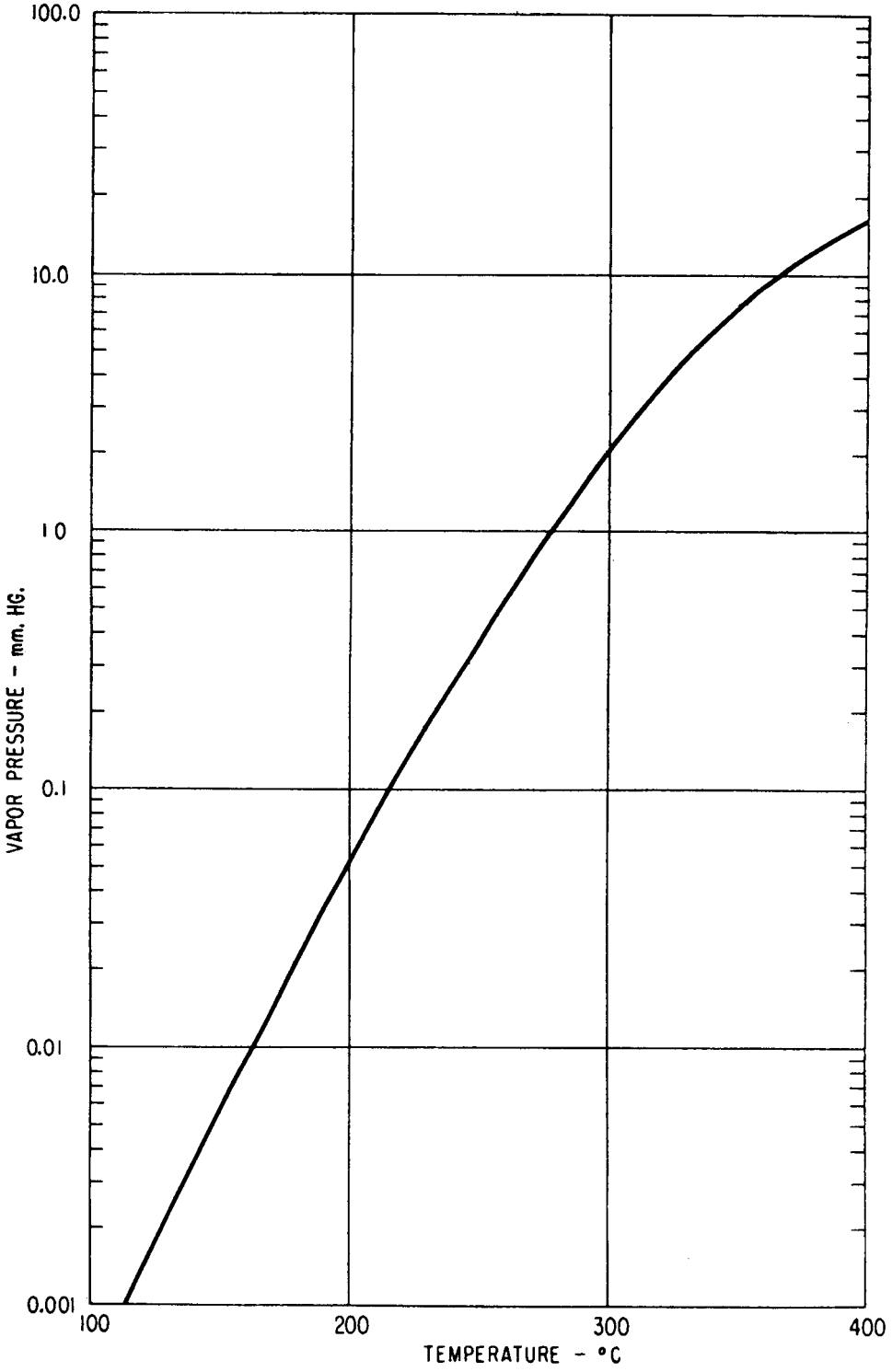

FIG. 18. The vapor pressure of cesium versus temperature.

broader when a thick channeled slit is used instead of a thin slit. It is presumed that the reason for this is that the thick slit concentrates more of the beam in a small solid angle about the normal. Slow atoms from the oven are selected by the deflecting fields only when they are emitted at relatively large angles from the normal. Ovens made of iron or stainless steel are popular, although copper and many other materials are quite likely to work satisfactorily.

VI. The Transition Process

In an atomic beam resonance experiment, the energy level scheme of the atom is determined by subjecting the beam to a radiation field. This field is applied in the C field region between the A and B deflecting magnets (see Fig. 8a). When the frequency of the radiation is swept through the frequency of an allowed transition, a change in moment of the atoms will occur. As a result of this moment change, the transverse force on the atoms in the second deflecting field also changes and a variation in detected beam current is observed.[8]

The width and intensity of the spectral lines—and consequently the transition probability as a function of frequency—are of considerable importance in the design, interpretation, and ultimate accuracy of an atomic beam experiment. The line width is given approximately by the Heisenberg relation:

$$\Delta\nu\tau \sim 1,$$

where $\Delta\nu$ is the line width and τ is the time the atom spends in the radiation field. In contrast with microwave absorption spectroscopy, collision and Doppler broadening can be made negligibly small in beam experiments. For purposes of atomic frequency standards, it is logical to choose states with long lifetimes so that the spectral line is not broadened by spontaneous emission processes.

The original Rabi method of exciting the atomic resonance employs a single oscillating field. In 1950, Ramsey introduced a method of excitation using two separated oscillating fields. There are a number of advantages to this method over the Rabi method. The Ramsey method improves the resolution of the spectrometer. It does not require as high a degree of uniformity of the static C field. It has a practical advantage when observing very high frequency transitions.[9] Two short oscillating fields separated by

[8] This is not strictly true. The moment of an atom as it passes through the A deflecting magnet will not differ from its moment in the B deflecting field for $\Delta F = 0$, $\Delta m_F = \pm 1$ ($m_F \neq I + \frac{1}{2}$) transitions if the deflecting fields are strong. Consequently, no change will be observed in the beam intensity when a transition of this type is induced (see Fig. 9).

[9] The oscillating field should be uniform in intensity and phase, and this is difficult to achieve when the oscillating field region is many free-space wavelengths long.

a distance L provide even higher resolution than a single ideal field covering the entire distance L. The advantage is gained at the expense of a reduction in signal-to-noise ratio that depends upon the velocity distribution in the beam.

A. The Transition Probability for a Single Oscillating Field

The Hamiltonian for an atom in the presence of a radiation field can be written as:

$$\mathcal{H}(t) = \mathcal{H}_0 + \mathcal{H}'(t), \tag{60}$$

where $\mathcal{H}_0$ is the Hamiltonian in the absence of the radiation field, and $\mathcal{H}'(t)$ is the interaction between the radiation field and the magnetic moment $\boldsymbol{\mu}$ of the atom. This second term may be written to sufficient approximation as

$$\mathcal{H}'(t) = -\boldsymbol{\mu} \cdot \mathbf{H} \cos \omega t, \tag{61}$$

where H is the magnitude of the oscillating magnetic field intensity and ω is the angular frequency of this oscillating field. In order to obtain the transition probability and the theoretical line shape, the time dependent Schrödinger equation must be solved. A complete solution may be obtained if certain assumptions are made. We will proceed to enumerate these assumptions.

(a) The two states involved in the transition are well isolated from other states.

(b) The diagonal elements of the interaction Hamiltonian are zero.

(c) The atom sees a finite portion of a cosine wave as it passes through the radiation field region. It enters the field at $t = 0$ and leaves at time τ. A substantial simplification can be made in the calculation without serious discrepancies in the results if it is assumed that the dipole moment interacts with a rotating field rather than an oscillating field. Instead of Eq. (61), write

$$\mathcal{H}'(t) = -\boldsymbol{\mu} \cdot (H \cos \omega t \mathbf{i} - H \sin \omega t \mathbf{j}), \tag{62}$$

where the z-axis is chosen along $\mathbf{H}_0$, the uniform C field, and H rotates with angular velocity ω in the x,y-plane. We have chosen the special case where the radiation field has a z-component equal to zero.

With these simplifying assumptions, the transition probability that an atom initially in state p, will be in state q after a time τ, is given by

$$P_{p,q}(\tau) = \frac{|2b|^2}{(\omega_0 - \omega)^2 + |2b|^2} \sin^2 \left\{ \frac{1}{2} [(\omega_0 - \omega)^2 + |2b|^2]^{1/2} \tau \right\}. \tag{63}$$

The quantity b is related to the matrix elements of the interaction Hamiltonian by

$$\mathcal{H}_{pq}' = \int \psi_p^* \mathcal{H}'(t) \psi_q d\tau = \hbar b e^{+i\omega t}, \tag{64}$$
$$\mathcal{H}_{qp}' = \int \psi_q^* \mathcal{H}'(t) \psi_p d\tau = \hbar b^* e^{-i\omega t},$$

and

$$\omega_0 = (W_q - W_p)/\hbar.$$

The maximum transition probability occurs at resonance ω_0 when b and τ are related by

$$|b|\tau = \frac{\pi}{2}$$

or

$$|b| = 1.57 \frac{v}{l} \tag{65}$$

where v is the velocity of the atoms, and l is the length of the oscillating field traversed by the atoms. The frequency width at half maximum for these optimum conditions is

$$\Delta\nu = 0.799 \frac{v}{l}. \tag{66}$$

If the velocity distribution of the atoms in the beam is taken into account (*6*, *7*)

$$|b| = 1.89 \frac{\alpha}{l} \tag{67}$$

where α is the most probable velocity in the source and the velocity distribution in the beam is assumed to be that for simple effusion through an ideal aperture. The line width in this case is

$$\Delta\nu = 1.07 \frac{\alpha}{l}. \tag{68}$$

The radiation field intensity required to produce the optimum transition probability is given by Eqs. (64) and (67). For the purpose of an estimate we make the following approximation. The radiation field interacts most strongly with the electronic magnetic moment, and we may write

$$\boldsymbol{\mu} = \boldsymbol{\mu}_J + \boldsymbol{\mu}_I \approx \boldsymbol{\mu}_J.$$

Then

$$\mathcal{H}'(t) = -\boldsymbol{\mu} \cdot (H \cos \omega t \mathbf{i} - H \sin \omega t \mathbf{j})$$
$$\approx g_J \mu_0 \mathbf{J} \cdot (H \cos \omega t \mathbf{i} - H \sin \omega t \mathbf{j}).$$

This can be rewritten as

$$\mathcal{H}'(t) = \frac{1}{2} g_J \mu_0 H [J_+ e^{i\omega t} + J_- e^{-i\omega t}],$$

where $J_\pm = J_x \pm iJ_y$. Now

$$2b = \frac{g_J \mu_0 H}{\hbar} \langle p|J_+|q\rangle = \frac{\mathcal{K}_{pq}' e^{-i\omega t}}{\hbar}, \tag{69}$$

and

$$2b^* = \frac{g_J \mu_0 H}{\hbar} \langle q|J_-|p\rangle = \frac{\mathcal{K}_{qp}'^* e^{i\omega t}}{\hbar}.$$

The nonvanishing matrix elements of J in the weak field representation (F, m_F) are (*28*)

$$\langle F, m_F|J_\pm|F, m_F \pm 1\rangle = A[(F \pm m_F)(F \mp m_F + 1)]^{1/2},$$
$$\langle F, m_F|J_z|F, m_F\rangle = Am_F,$$

where

$$A = \frac{J(J+1) - I(I+1) + F(F+1)}{2F(F+1)};$$

$$\langle F, m_F|J_\pm|F+1, m_F \pm 1\rangle = \pm B[(F \mp m_F + 1)(F \mp m_F + 2)]^{1/2},$$
$$\langle F, m_F|J_z|F+1, m_F\rangle = B[(F+1)^2 - m_F^2]^{1/2},$$

where

$$B = \left[\frac{(F+1-J+I)(F+1+J-I)(J+I+2+F)(J+I-F)}{4(F+1)^2(2F+1)(2F+3)}\right]^{1/2}; \tag{70}$$

$$\langle F, m_F|J_\pm|F-1, m_F \pm 1\rangle = \mp C[(F \pm m_F)(F \pm m_F - 1)]^{1/2},$$
$$\langle F, m_F|J_z|F-1, m_F\rangle = C[F^2 - m_F^2]^{1/2},$$

where

$$C = \left[\frac{(F-J+I)(F+J-I)(J+I+1+F)(J+I+1-F)}{4F^2(2F-1)(2F+1)}\right]^{1/2}.$$

The selection rules $\Delta F = 0, \pm 1$; $\Delta m_F = 0, \pm 1$ are derived from these matrix elements.

If the C field is very weak, as it is in atomic frequency standards, then the matrix elements (70) may be used directly in Eq. (69). In the event that there is a component of the radiation field in the z-direction—contrary to the assumption made in writing Eq. (62)—the matrix elements of J_z are necessary in calculating the transition probability. The $(F = 4, m_F = 0) \leftrightarrow (F = 3, m_F = 0)$ transition in cesium is a case in point.

Torrey has given a useful approximate evaluation of b for general values of the C field intensity (*29*). For π-transitions,

$$2b = \frac{2}{\hbar} H_x \left[\left(\frac{g_J \mu_0}{2} \pm \mu_{F,m_F}\right)\left(\frac{g_J \mu_0}{2} \mp \mu_{F',m_F \pm 1}\right)\right]^{1/2}, \tag{71}$$

where H_x is the component of the radiation field perpendicular to $\mathbf{H}_0$, and μ_{F,m_F} are the magnetic moments of the states F, m_F. These effective magnetic moments are given by

$$\mu_{I\pm\frac{1}{2},m_F} = \mp \left\{ \frac{x + (2m_F/2I+1)}{[1 + (4m_F x/2I+1) + x^2]^{\frac{1}{2}}} \right\} \frac{g_J \mu_0}{2},$$

if $m_F \neq \pm(I + \frac{1}{2})$, and

$$\mu_{I+\frac{1}{2},m_F} = \mp \frac{g_J \mu_0}{2},$$

if $m_F = \pm(I + \frac{1}{2})$.

For σ-transitions,

$$2b = -\frac{\mu_0}{\hbar}(g_J - g_I)\left[1 - \left(\frac{2m_F}{2I+1}\right)^2\right] \frac{H_z}{[1 + (4m_F x/2I+1) + x^2]^{\frac{1}{2}}}. \quad (72)$$

If g_I is neglected relative to g_J then,

$$2b = -\frac{2H_z}{\hbar}\left[\left(\frac{g_J \mu_0}{2}\right)^2 - (\mu_{F,m_F})^2\right]^{\frac{1}{2}}. \quad (73)$$

H_z is the component of the radiation field parallel to $\mathbf{H}_0$, and the quantity x has its previous value:

$$x = \frac{(g_J - g_I)\mu_0 H_0}{\Delta W}.$$

When there is a component of the radiation field in the direction of $\mathbf{H}_0$, the diagonal matrix elements of the interaction Hamiltonian do not vanish and one of the assumptions (b) used in the derivation of Eq. (63) is violated. If, however, $|\mathcal{H}_{pp'}|$ and $|\mathcal{H}_{qq'}| \ll h\omega_0$, which they are for the standard frequency transition, then Eq. (63) still provides a reasonably good approximation.

A more exact treatment of the transition probability for π-transitions using the rotating field approximation is given by H. Salwen (*11*, *30*). Salwen's theory includes the interaction between neighboring states. Small frequency shifts in the resonances result. Salwen makes the additional assumption that the widths of allowed lines are small compared to their separations. The analysis has not been made for σ-transitions which are of particular interest in atomic beam standards. The significance of these frequency shifts predicted by Salwen can be demonstrated by looking for a displacement of the resonance peak as a function of radiation field intensity. If a shift is not observable within the precision of measurement over a range of oscillator field intensity, then the frequency shifts are not significant in the measurements. Of course, radiation field dependent frequency

shifts can, and frequently do, result from instrumental difficulties quite apart from the effects produced by neighboring states in the spectrum.

Oscillating fields rather than rotating fields are employed in atomic beam experiments. Even when the effects of neighboring states are neglected, an oscillating field will produce a small shift in frequency which is not predicted by the rotating field approximation. An oscillating field solution to the time dependent wave equation was first obtained by Bloch and Siegert (*31*) for particles of spin ½. In their calculation it was assumed that the magnitude of the radiation field H is small compared to the uniform C field H_0 and that $\mathbf{H}$ and $\vec{\mathbf{H}}_0$ are perpendicular to each other. They calculated the frequency shift to be

$$(\nu_0' - \nu_0) = \frac{\nu_0}{16}\left(\frac{H}{H_0}\right)^2, \tag{74}$$

where ν_0' is the frequency at the peak of the resonance curve and ν_0 is the frequency separation of the two states. This relationship probably applies satisfactorily to the $\Delta F = 0$, $\Delta m_F = \pm 1$ transitions in the cesium standard provided that care is taken to keep H small relative to H_0. An estimate of this frequency shift for $\Delta F = \pm 1$, $\Delta m_F = \pm 1$ transitions can be made by inserting the value of the magnetic field at the position of the nucleus into (74) for H_0 rather than the magnitude of the C field intensity. This field is 3.3×10^6 oe for cesium. The theoretical analysis of the oscillating field induced $\Delta F = \pm 1$, $\Delta m_F = 0$ transitions has not been performed.

B. The Transition Probability for Two Separated Oscillating Fields (7)

In the Ramsey method of excitation, the beam passes through two separated oscillating fields contained within the uniform C field. The probability that an atom, initially in state p, will be in state q after passing through both oscillating fields is given by

$$P_{p,q} = 4\sin^2\theta\,\sin^2\frac{a\tau}{2}\left[\cos\frac{1}{2}(\lambda T - \delta)\cos\frac{a\tau}{2} - \cos\theta\sin\frac{1}{2}(\lambda T - \delta)\sin\frac{a\tau}{2}\right]^2, \tag{75}$$

where

$$\sin\theta = \frac{|2b|}{a}, \qquad \cos\theta = \frac{\omega_0 - \omega}{a},$$

$$a = [(\omega_0 - \omega)^2 + |2b|^2]^{1/2},$$

$$\omega_0 = \frac{W_q - W_p}{\hbar},$$

$$\lambda = \frac{\bar{W}_q - \bar{W}_p}{\hbar} - \omega,$$

τ is the time taken by an atom to pass through either of the two oscillating fields of length l, T is the time taken by an atom to traverse the distance L between the two fields,

$$\tau = \frac{l}{v}, \qquad T = \frac{L}{v},$$

and b is given by Eqs. (64) and (69). It is assumed, as for Eq. (63), that $\mathcal{H}_{pp'} = \mathcal{H}_{qq'} = 0$. The second oscillating field leads the first by the phase angle δ. $\bar{W}_p$ and $\bar{W}_q$ are the average energies of states p and q in the region between the two fields.

The transition probability, Eq. (75), provides the theoretical line shape for a single velocity beam. A probability of one is obtained at $\omega = \omega_0$ when $\delta = 0$ and $b\tau = \pi/4$. When $P_{p,q}$ is averaged over the velocity distribution of a beam effusing from an ideal aperture, the maximum transition probability is given at $\omega_0(\delta = 0)$ when

$$b = 0.942\,\frac{\alpha}{l}. \tag{76}$$

Notice that the field intensity required is about half that required for the optimum condition for a Rabi flop in an oscillating field of length l.

The halfwidth of the central peak of the Ramsey pattern is

$$\Delta\nu = 0.64\,\frac{\alpha}{L} \tag{77}$$

under the conditions of Eq. (*76*). The form of the Ramsey pattern is shown in Fig. 19. The pedestal upon which the interference pattern sits is usually much broader than the interference pattern. In some cases the pedestal width is over 700 times the width of the central peak. The minima of the Ramsey transition probability would decrease all the way to zero in the case of a single velocity beam. A distribution in velocity of the atoms tends to smooth out the interference pattern. Greater smoothing action occurs at larger frequency displacements from the central resonance peak.

When the phase of the second oscillating field leads that of the first by $\delta = \pi$ radians, a minimum occurs at ω_0 rather than a maximum (see Fig. 19b). When $\delta = (\pi/2)$, the transition probability takes the form of a dispersion curve about ω_0 (see Fig. 19c). It is evident that if a small phase difference exists ($\delta \neq 0$) between the two fields, the peak of the resonance will be shifted in frequency relative to ω_0. An apparent frequency shift arising from a phase difference between the oscillating fields can be, and frequently is, significant in atomic beam frequency standards.

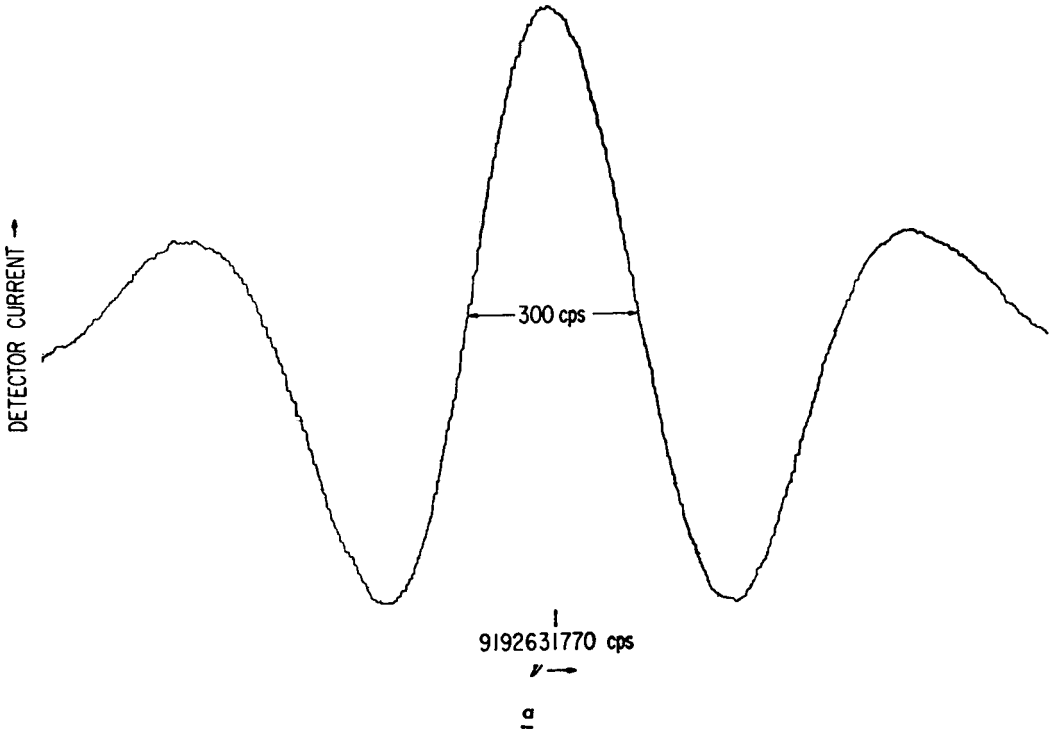

FIG. 19a. An actual trace of a Ramsey interference pattern when the two oscillating fields are in phase.

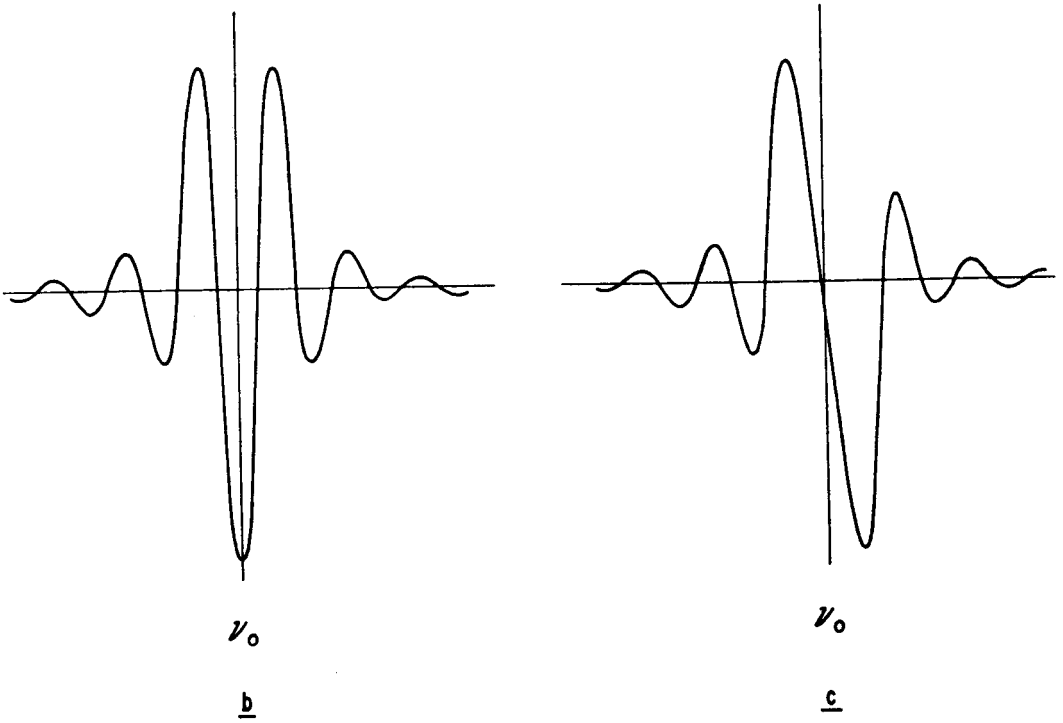

FIG. 19. (b) The form of the Ramsey pattern when the oscillating fields differ in phase by 180°. (c) The form of the Ramsey pattern when the oscillating fields differ in phase by 90°.

VII. Measurement Uncertainties

There are a number of uncertainties introduced into the absolute frequency measurements of a cesium standard. The ideal circumstance, of course, is to have the accuracy of these devices limited only by the random scatter in the data—all systematic frequency shifts having been measured or eliminated. Ideally then, the accuracy would be determined by the spectral line width and signal-to-noise ratio. At the present time systematic

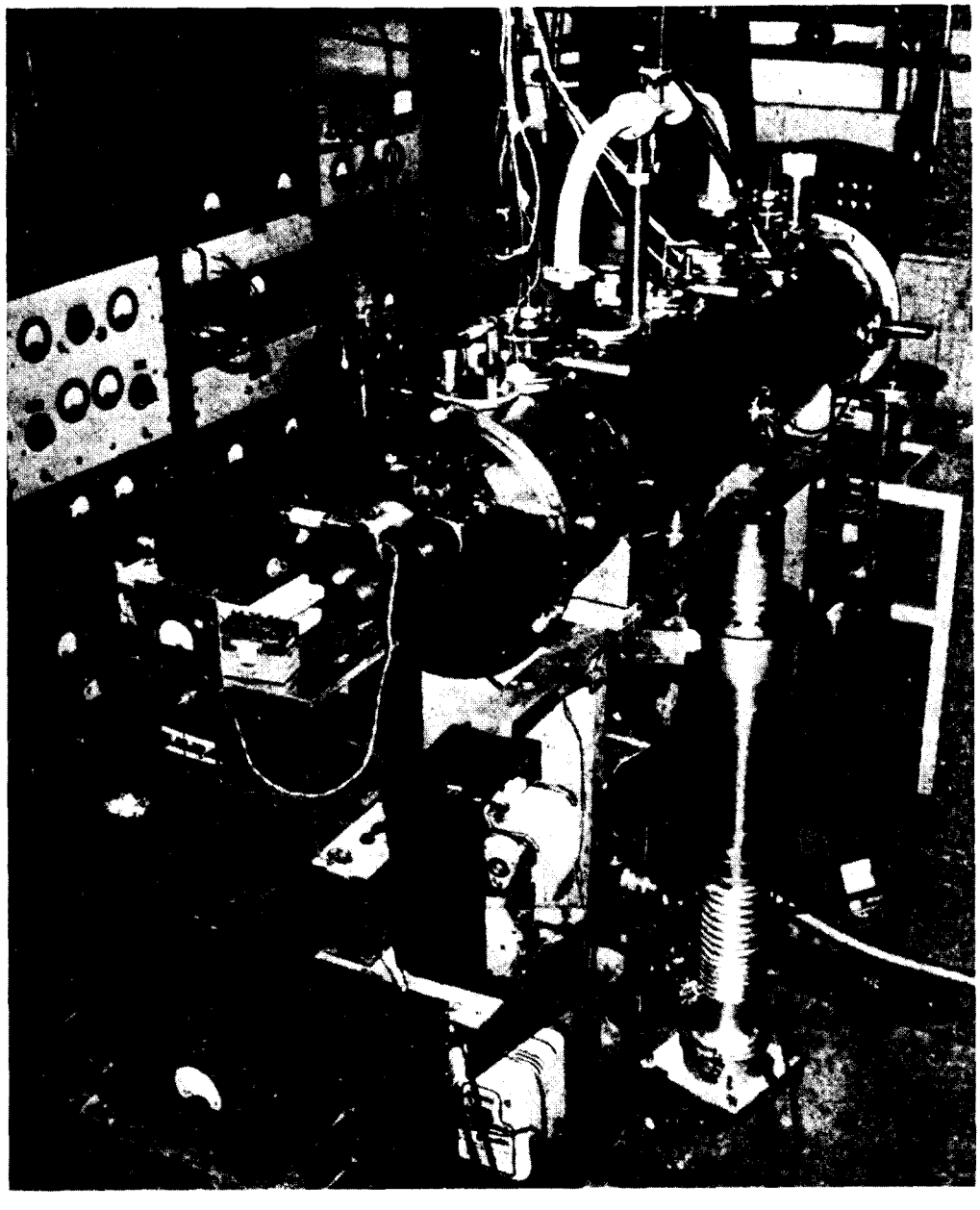

Fig. 20. NBS-I atomic beam frequency standard.

errors do limit the accuracy of cesium frequency standards. Beam devices with 300 cps line widths have demonstrated greater accuracy than those devices with much narrower resonances. As time progresses it is expected that longer machines will more closely approach their ideal capabilities.

Certain fixed parameters and effects that determine absolute frequency may be measured by auxilliary experiments. The effects that are now considered to contribute the greatest inaccuracies are:

(a) The magnitude and nonuniformity of the C field, including variations in the magnitude over long periods,

(b) A phase difference between the two oscillating field regions, and

(c) A lack of purity of the electromagnetic field exciting the atomic transition.

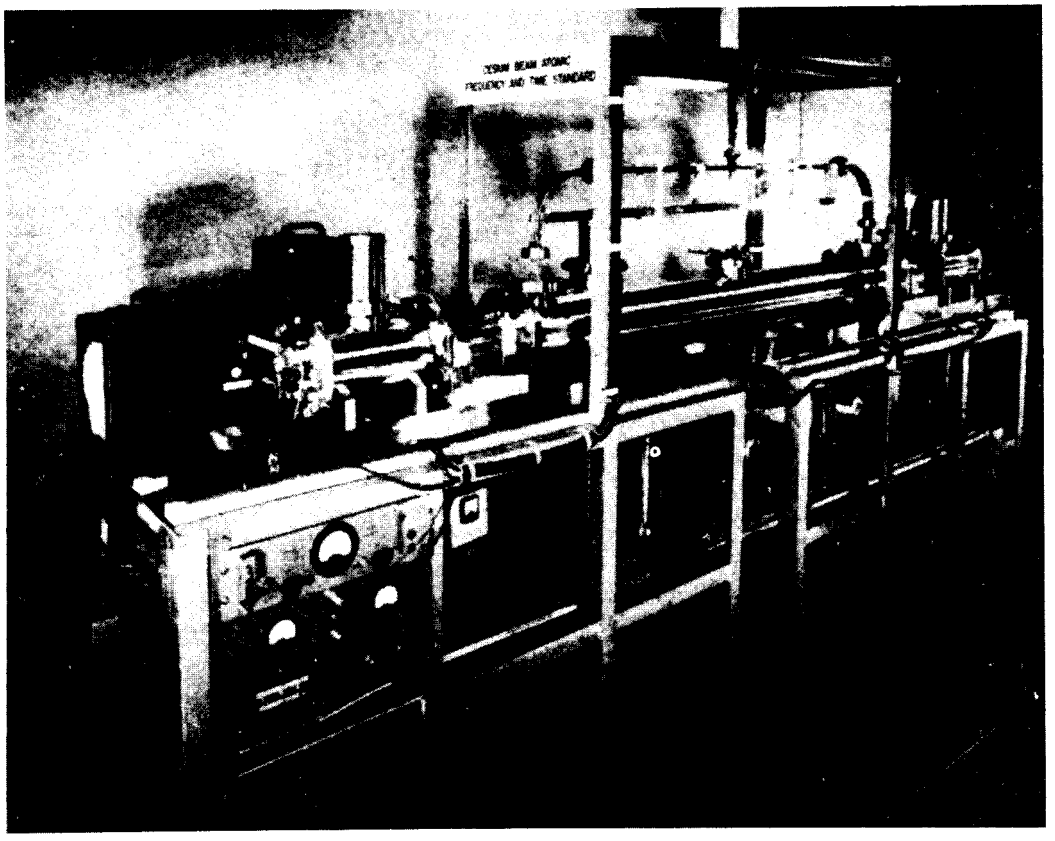

FIG. 21. NBS-II atomic beam frequency standard.

The method of measuring these effects and the results of the measurements together with the estimated uncertainty in absolute frequency will be presented for the United States Frequency Standard and alternate standard (see Mockler, *1*, *32*, *33*). The two devices are designated (NBS-II) and (NBS-I) respectively. They are shown in Figs. 20 and 21; their properties are given in the Appendix.

A. Magnetic Field Measurements

The magnitude of the C field is determined by observing a number of field sensitive microwave transitions, e.g., $(F = 4, m_F = \pm 1) \leftrightarrow (F = 3, m_F = \pm 1)$. The frequencies for these transitions are given by Eq. (24) which can be written to sufficiently good approximation as:

$$\nu = \nu_0 + 700.6 m_F \bar{H}_0, \tag{78}$$

where ν_0 is the hyperfine structure separation in zero field. The quantities ν and ν_0 are measured in kilocycles and $\bar{H}_0$ in oersteds.

The low frequency transitions for which $\Delta F = 0$, and $\Delta m_F = \pm 1$ are also used to measure the magnitude of the field and, in addition, the uniformity of the field. The frequency of these transitions is given by Eqs. (25) and (26). The abbreviated equation

$$\nu = 350 \bar{H}_0 \tag{79}$$

is a satisfactory approximation. The quantity ν is measured in kilocycles and $\bar{H}_0$ in oersteds. Small coils were placed at various positions (5 altogether) along the C field. The magnitude and uniformity of $\bar{H}_0$ is obtained by exciting each coil separately. A rotating coil fluxmeter, sensitive to 0.002 oe, provides still another method of measuring the field and its uniformity.

The uncertainty in the field measurements of amount δH_0 will produce an uncertainty in the standard frequency measurement given by

$$\delta \nu_0' = 854 H_0 \delta H_0; \tag{80}$$

$\delta \nu_0'$ is measured in cps and the field in oersteds. One would expect the average field $\bar{H}_0$ obtained from the microwave measurements to agree with the average of the local field measurements made at low frequencies and with the rotating coil fluxmeter, provided, of course, that a sufficient number of points are chosen along the field to give a good average. In NBS-I this is the case. The fields measured in the various ways agree within the precision of measurement. The maximum deviation in the C field in this instrument is ± 0.002 oe. In NBS-II there is a measured discrepancy of 0.004 oe in the average field measurements made by the different methods. This is still unexplained but seems to be associated with a deteriorating of the shielding properties of the μ-metal shields used to eliminate the earth's field, the fringing fields of the deflecting magnets, and other stray fields in the laboratory. When the shields were first installed there was no discrepancy between the various field measurements.

The average value of the square of the C field magnitude must be known in order to calculate the frequency ν of the peak of the resonance

curve and consequently the frequency of the exciting radiation at this point. It is obtained from Eq. (23) which can be written to sufficient approximation as:

$$\nu = \nu_0 + 427\overline{H_0^2}, \tag{81}$$

where ν and ν_0 are in cps and H_0 in oersteds. The zero field hyperfine separation, ν_0, is assumed to be 9192631770.0 cps for this calculation. The number 9192631770 $\pm$ 20 cps is the best value of ν_0 from astronomical time measurements as determined by Markowitz *et al.* (*5*). Additional significant figures are added simply to accommodate the additional stability of the atomic standards.

The average value of the field squared may be different from the square of the average field. Consequently, if the C field is not uniform, the low frequency measurements of H_0 at a sufficient number of points, n, would give the best value of $\overline{H_0^2}$. Using these data,

$$\overline{H_0^2} = \frac{1}{n}\sum_{i=1}^{n} H_{0i}^2,$$

where H_{0i} is the average field measured by the sensing coil at the ith position in the C field. The low frequency spectral line is subject to distortion and power shifts. Care must be taken to maintain the radiation field intensity H small compared to H_0 to avoid these "saturation" effects. Even at these low frequencies (7 to 21 kc) the Bloch-Siegert effect, Eq. (74), is unimportant (4–13 cps) insofar as the field measurements are concerned.

B. Phase Difference Errors

If the two oscillating fields of the Ramsey excitation structure are in phase, a maximum beam signal is observed at the resonance frequency. If the two fields are 180° out of phase, a minimum signal is observed at the resonance frequency. The central peak is shifted approximately a fringe width as the phase difference is shifted from 0° to 180°. Then if the width of the fringe is 120 cps, a phase difference of 1° will shift the frequency about 0.7 cps which is significant.

For the purpose of reducing the phase difference between the two fields, it was found quite effective to pass the beam through the two ends of a single rectangular resonant cavity electroformed in the shape of a *U*. The beam grazes the two end walls. The cavity is driven by the frequency multiplier chain through a coupling iris at the midpoint of the U. The cavity is made so that it may be rotated 180°, thus reversing the direction of traverse of the beam through the exciting structure. The frequency shift accompanying any phase difference will be in opposite directions for the

two orientations. The mean of the two frequencies is the line frequency and one-half the difference is the phase correction. Simple relationships for estimating this frequency shift from the plotted Ramsey pattern have been developed by Holloway *et al.* (*34*). Their method is less sensitive than the more common method of exchanging the oscillating fields.

C. Errors Resulting from Impure Radiation

The simple theory of spectral line shape assumes the atomic transition to be excited by pure sinusoidal or cosinusoidal radiation. If the electromagnetic field is not pure, rather large frequency uncertainties are possible in the measurements. Actually, of course, the transition is induced by a certain distribution of frequencies. This distribution is determined by the frequency multiplier and crystal oscillator from which the exciting radiation is derived. The radiation, in general, is composed of the carrier frequency, noise and discrete sidebands resulting from frequency modulation. The discrete sidebands are usually due to 60 cps—the power frequency—and multiples thereof. (In the cesium beam experiments it is possible to reduce the noise to a low enough level so that it is not the limiting factor in the precision of the frequency measurements). The sidebands are multiplied in

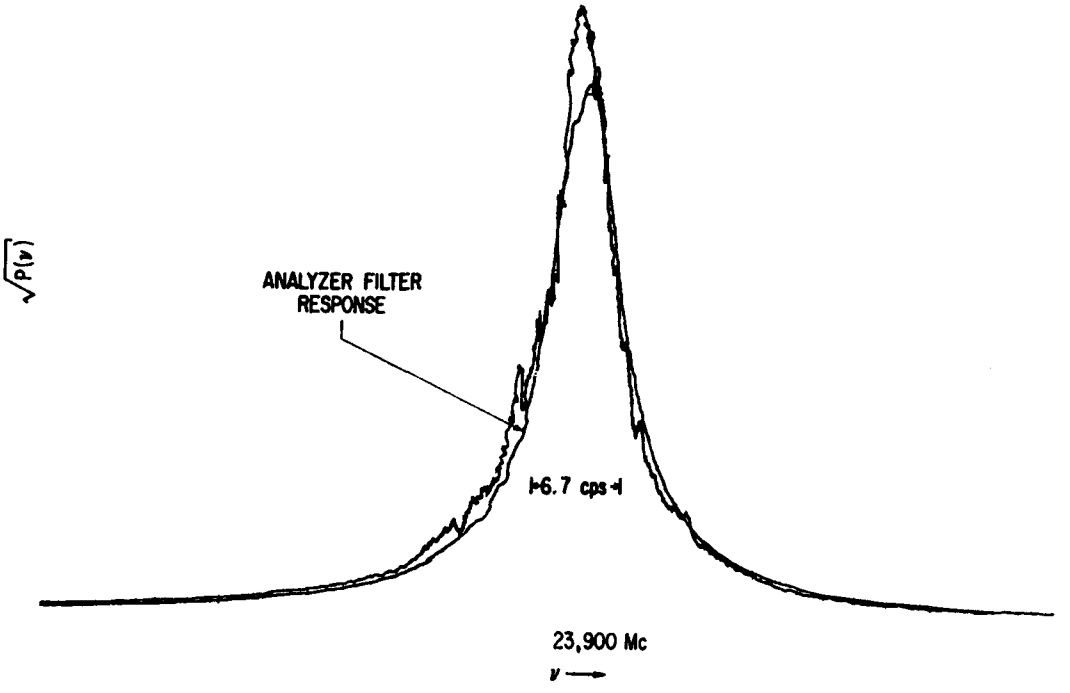

FIG. 22. The square root of the power spectrum of a 5 Mc quartz crystal oscillator multiplied in frequency to 23,900 Mc. This oscillator is used in the excitation chain of the United States Frequency Standard. The width and shape of the spectrum is essentially that of the response of the analyzing filter.

intensity by the factor of frequency multiplication. This factor is rather large (1836) and consequently these sidebands can introduce rather large frequency errors. Errors of this sort are particularly significant if the power spectrum is unsymmetrical.[10] Frequency shifts of a few parts in 10^9 have been observed by deliberately introducing sidebands unsymmetrically placed about the carrier.

Of course, if the power spectrum is known, the proper spectral line shape can be calculated in order to find the proper correction to the measured

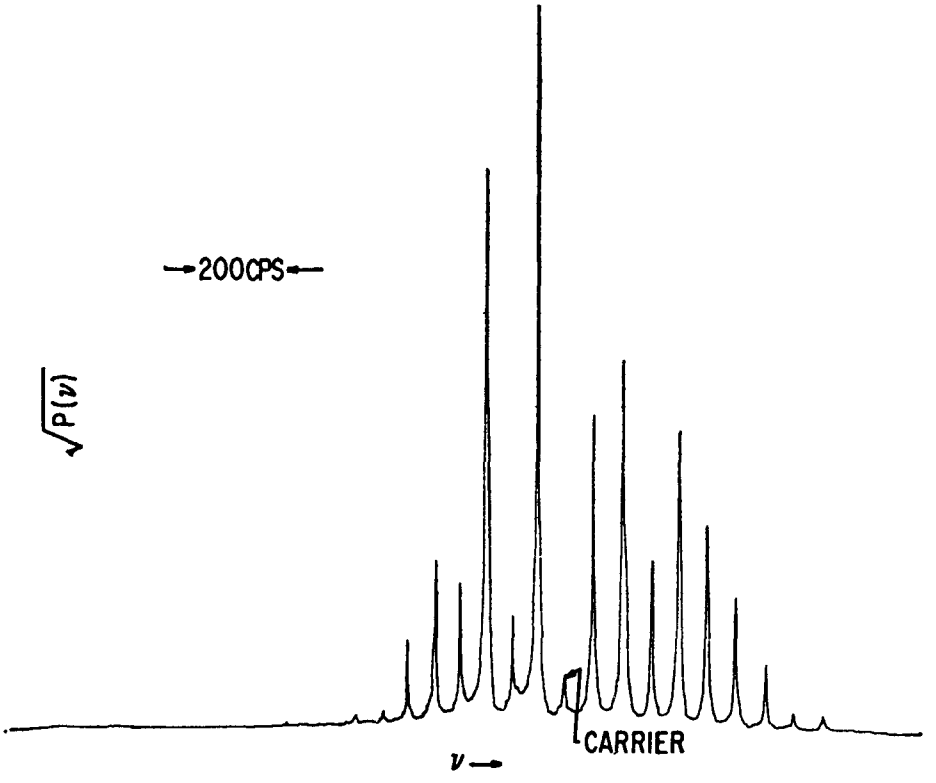

FIG. 23. The square root of the power spectrum of a 10 Mc quartz oscillator multiplied, in effect, to 15,000 Mc. Notice the 60 cps sidebands. The crystal in this oscillator is immersed in liquid helium.

frequency. It is both more desirable and much simpler to eliminate these sidebands so that the simple line shape theory applies. The square root of the power spectrum of a 5 Mc quartz crystal oscillator multiplied in frequency to 23,900 Mc is shown in Fig. 22. This is the oscillator used in the excitation chain of the United States Frequency Standard. Considerable care was taken with this oscillator to avoid 60 cps modulation. It was found necessary to use regulated dc power supplies in the filament circuits both

[10] An unsymmetrical power spectrum can arise when the carrier is frequency modulated with two or more different frequencies (*35*).

463-560 O - 72 - 5

in the oscillator and the frequency multiplier chain. Figure 23 plots the square root of the power spectrum of a similar oscillator circuit without regulation of the filament supply. The 60 cps sidebands are very prominent. Notice that the spectrum is quite unsymmetrical. In this spectrogram the 10 Mc oscillator was multiplied to 15,000 Mc.

The spectra of Figs. 22 and 23 were taken by means of an ammonia maser spectrum analyzer (*36*, *37*) developed by James Barnes and others in the Atomic Frequency and Time Standards Section of the National Bureau of Standards. The smooth trace in Fig. 22 is the response curve of the analyzer filter. It has been offset and reduced in intensity relative to the oscillator spectrum so that the two would not coincide. The resolution is insufficient to see the details of the spectrum. It can be said, however, that the spectrum has a width of 1 cps or less at 23,900 Mc. This is sufficiently narrow to assume that the cesium transition in the frequency standard is excited by a pure signal.

Low frequency crystal oscillators, for example, 100 kc oscillators, in most cases are unsuitable for exciting the cesium transition. The huge factors of frequency multiplication usually give power spectral widths greater than 1 kc at the cesium frequency. This is greater than the width of the cesium line. Ramsey (*7*, *38*) has considered the frequency shifts produced by exciting a transition with two or more signals close to each other.

D. Other Errors

The peak of the Ramsey pattern may be incorrectly determined if it is measured against a variable background of intensity. The cesium spectrum is essentially symmetrical about the $(F = 4, m_F = 0) \leftrightarrow (F = 3, m_F = 0)$ transition and overlap errors will tend to cancel. There may be, however, geometrical effects in the spectrometer that reduce the intensity of certain lines in the spectrum relative to their symmetrically placed counterpart. This would lead to an overlap error. The relative intensities of the lines on the high and low frequency side of ν_0 have been measured. The intensities of the $(F = 4, m_F = 1) \leftrightarrow (F = 3, m_F = 1)$ and $(F = 4, m_F = -1) \leftrightarrow (F = 3, m_F = -1)$ lines are found not to be the same but differ by about 25%. This leads to a calculated overlap error of about 1×10^{-12} at usual C field intensities. This estimate takes into account only superposition of the various lines of the spectrum. Lower fields will introduce still smaller errors. Transitions for which $\Delta m_F = \pm 1$, that is, π-lines, are not observable in the NBS standards and were not considered in the calculated estimate.

Saturation effects are thought not to contribute significantly to the frequency error because no frequency shifts were observable as the radiation field intensity was changed from very small values to rather large

values.[11] Beyond the values used, the line intensity was either too low or the line too broad for precise measurements. The problem of saturation as it applies to σ-transitions and the effect of the oscillating field in shifting the line frequency requires further theoretical study.

One would expect first order Doppler effects to broaden the spectral line by an unimportant amount. It is conceivable, however, that the small holes in the resonant cavity through which the beam passes radiate different amounts of energy. The entrance holes radiate differently than the exit holes. This radiation, though small, will be propagated against the beam from the entrance holes and in the direction of the beam from the exit holes. If both sets of holes radiate in the same way, the Doppler effect will broaden the line symmetrically. If they do not radiate in the same way the resonance peak will be shifted. A shift of this sort should be observable by rotating the waveguide exciting structure. It could be distinguished from a phase shift by changing the size of the holes. If the shift were very large, it would probably depend upon the radiation field intensity. No frequency shifts behaving in this way have been observed in the NBS standards.

Second order Doppler effect would introduce a fractional frequency shift of amount

$$\frac{\delta\nu}{\nu} = \frac{1}{2}\frac{\alpha^2}{c^2} \approx 5 \times 10^{-13},$$

where α is the most probable velocity of the atoms. This is a negligible shift for present experiments. Small but negligible frequency shifts arise from electric fields that might exist in the resonance excitation region. Haun and Zacharias (*39*) determined this shift experimentally and found it to be

$$\delta\nu_0 = 1.89 \times 10^{-6}\, E^2 \text{ cps},$$

where E is the electric field in volts/cm. For a field of 1 volt/cm,

$$\frac{\delta\nu_0}{\nu_0} = 2 \times 10^{-16}.$$

Frequency shifts incurred through frequency pulling of the resonant cavity are given approximately by

$$\Delta\nu_R = \left(\frac{Q_{\text{cavity}}}{Q_{\text{line}}}\right)^2 \Delta\nu_c$$

where $\Delta\nu_R$ is the shift in the peak of the atomic resonance line, and $\Delta\nu_c$ is the difference in frequency between the peak of the cavity response and the

[11] Relatively large saturation shifts are observed for π-transitions which are expected (*11*, *30*). These saturation shifts are also observed for σ-transitions if $m_F \neq 0$. The measured saturation shifts for the π transitions do not agree satisfactorily with Salwen's analysis.

peak of the spectral line. The estimated frequency shift from this source is about 4×10^{-14}.

E. Frequency Measurements

The fractional accuracy of the beam standard will be taken as the uncertainty in measurement of the Bohr frequency ν_0 relative to ν_0, i.e., $\delta\nu_0/\nu_0$. We suppose that ν_0 may have any number of significant figures required, so that the accuracy as defined here is limited only by the atomic standards themselves and not by inaccuracies in astronomical time measurements. Precision, on the other hand, will be understood to mean simply reproducibility. For example, if a fixed unknown phase difference exists between the two oscillating fields, the precision may be quite good but the accuracy is limited by the unknown phase shift.

An estimate of the fractional accuracy of a particular machine may be made by adding all of the experimentally determined fractional uncertainties contributed by the various effects considered in the preceding subsections of Section VII. Thus for NBS-II the uncertainty in the C field measurements introduces a frequency uncertainty of $\pm 8 \times 10^{-12}$, and the uncertainty in frequency due to a phase shift is $\pm 2 \times 10^{-12}$. Other effects discussed previously are expected to be negligible, or calculable. The estimate of the fractional accuracy is the sum or $\pm 1.0 \times 10^{-11}$ for NBS-II.

The uncertainty in the C field measurements of NBS-I give a frequency uncertainty of 4×10^{-12}. The uncertainty due to a phase shift is $\pm 2 \times 10^{-12}$, and the estimate of accuracy for NBS-I is 6×10^{-12}. There is a measurable phase error in NBS-I of 8×10^{-12}, however, this is a measurable shift and may be introduced as a correction. For one orientation of the NBS-I cavity the two devices disagree by 1.0×10^{-11}, and for the other orientation they disagree by 2.5×10^{-11}. The corrected measured zero field difference is 1.7×10^{-11}, which agrees with the sum of the individual estimates of accuracy for the two machines within the precision of measurement, which is 2×10^{-12}. These two standards are evidently limited in their accuracy by systematic errors and not by their line breadths, which are about 300 cps and 120 cps.

Comparisons between certain Atomichrons and the atomic frequency standard of the United Kingdom carried on at the National Physical Laboratory are discussed by Holloway *et al.* (*34*, *40*) and by McCoubry (*41*). Comparisons made through propagation data are given in Section VIII. Figure 24 shows a sample set of comparisons between NBS-I and NBS-II. The oscillator was noticeably more unstable the last half of the day for the measurements made in Fig. 24. This oscillator was less stable on this particular day than usual during the spring of 1960. The precision cited in the figure for the day's measurements is considered the standard

deviation of the mean which is

$$\sigma_M = \frac{1}{\nu_0}\left[\sum_{i=1}^{n} \frac{(\Delta\nu_i - \overline{\Delta\nu})^2}{n(n-1)}\right]^{1/2}.$$

The quantity $\Delta\nu_i$ is the ith measurement of the zero field frequency difference between the two standards, $\overline{\Delta\nu}$ is the average frequency difference and n is the total number of sets of measurements. For one method of comparison, see Mockler *et al.* (*1*). For the frequency multiplier chain circuits, see Schafer and Salazar (*42*). The circuits employed in the United Kingdom Standard are given by Essen and Parry (*43*).

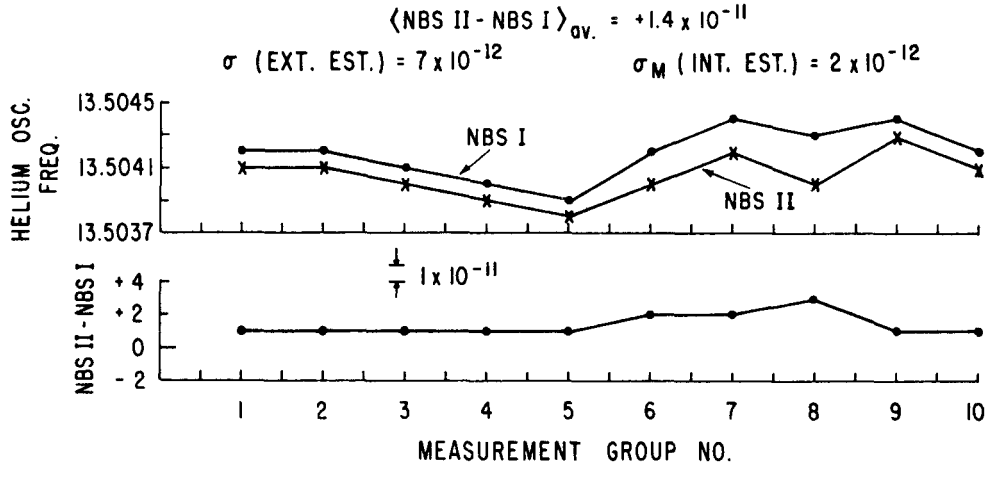

FIG. 24. A comparison of two cesium beam standards (NBS-I and NBS-II) by measuring the frequency of the same helium cooled crystal oscillator—one day's measurements. The crystal oscillator was unstable the last half of the day.

One method of measuring the frequency of a crystal oscillator in terms of the cesium resonance is shown in Fig. 25. This is the particular arrangement presently used with the United States standards. The ammonia maser stabilized crystal oscillator provides the most stable source for exciting the cesium transition that has been devised by the group. Other signal generators can be compared with this oscillator or with any signal output from either of the frequency multiplier chains for purposes of calibration. Also, any 5 Mc signal generator of sufficient stability may be used to drive the cesium beam chain directly for purposes of comparison with the cesium resonance.

It may prove practical to control the maser stabilized chain controlling the cesium excitation with a correction signal from the cesium beam. Thus the complete standard would be composed of an ammonia maser that would

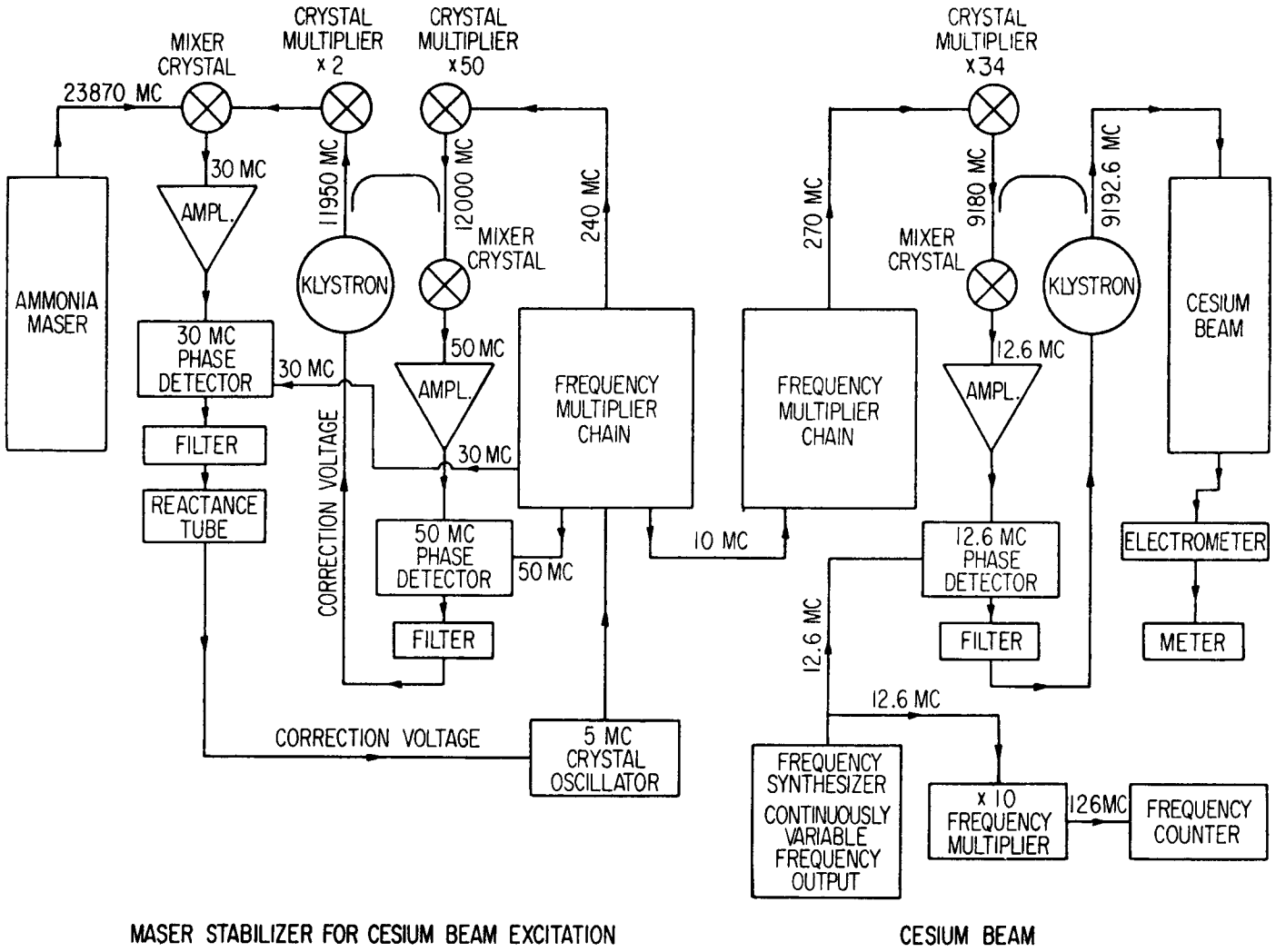

FIG. 25. A block diagram of the method of measuring the frequency of a crystal oscillator in terms of the cesium resonance used at the National Bureau of Standards. The crystal oscillator driving the cesium beam frequency multiplier is stabilized by an ammonia maser.

provide short term stability and the cesium beam which would determine the long term stability. If this device were operated continuously, and suitable scalars were added to accumulate cycles at, say, 5 or 10 Mc, then the device could properly be called an atomic clock.

VIII. Standard Frequency Comparisons between Cesium Standards via Propagation Data

Comparisons have been made through propagation data between the United States Frequency Standards, the United Kingdom standard at the National Physical Laboratory and four Atomichrons in the United States. The propagation data was obtained from the regular reports of: S. N. Kalra of the National Research Council of Canada; J. R. Pierce of the Cruft Laboratories; National Bureau of Standards Boulder Laboratories; Naval Research Laboratory, Washington, D. C.; and National Physical Laboratory, Teddington, England. The results are compiled in Table I. In this table the designation M_4 is the mean of the zero field frequencies of Atomichrons 106, 109, 110, and 112. The locations of these Atomichrons are indicated in the table.

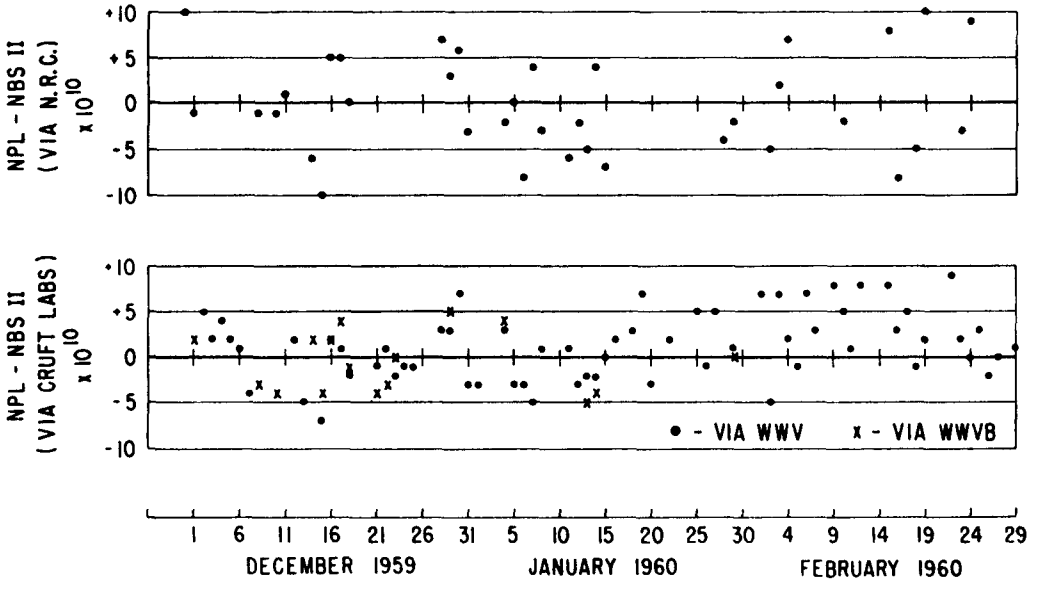

Fig. 26. Comparison of the United States Frequency Standard with that of the United Kingdom Standard using propagation data obtained from two different transmission links.

Figures 26 and 27 plot some of the data used in Table I and are given in order to display the scatter in the measurements. Figure 28 summarizes the propagation data available to date in terms of monthly averages.

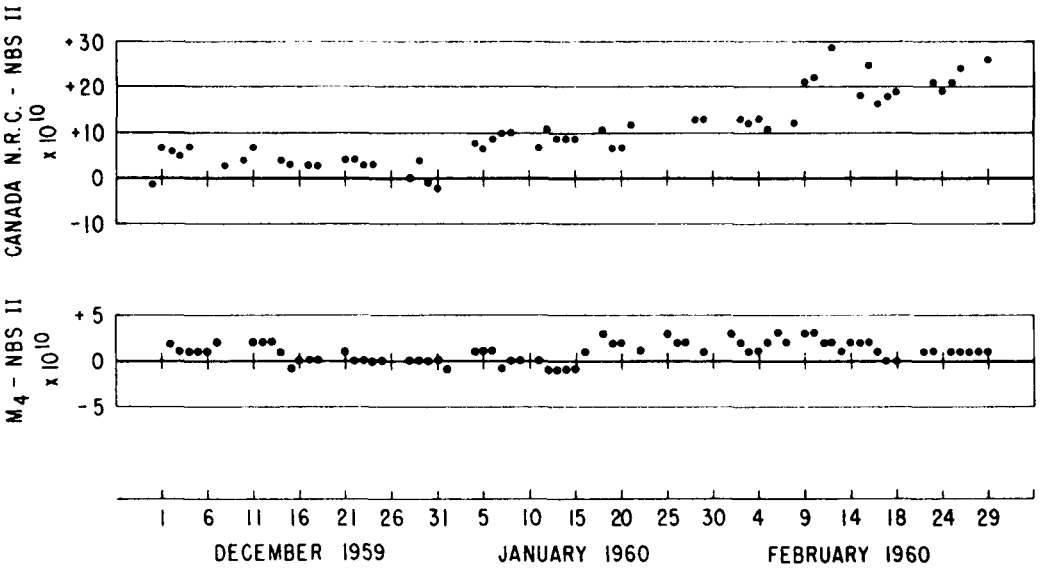

FIG. 27. Comparison of the United States Frequency Standard with that of Canada and with M_4.

TABLE I. SUMMARY OF 7-MONTH COMPARISONS BETWEEN NBS-II AND NPL, N.R.C. (CANADA), AND A GROUP OF 4 ATOMICHRONS[a]

Comparison	Number of daily comparisons used	Links used in the comparison
$(\text{NPL-NBS II})_{av} = +0.6 \times 10^{-10}$ via N.R.C. (Canada)	96	a. WWVB-NBS II b. WWVB-N.R.C. c. MSF-N.R.C. d. MSF-NPL
$(\text{NPL-NBS II})_{av} = +1.2 \times 10^{-10}$	128	a. 106-NBS II b. WWV-106—(30 day averages) c. WWV-112 d. MSF-112 e. MSF-NPL
$(\text{N.R.C.-NBS II})_{av} = +4.7 \times 10^{-10}$	128	a. WWVB-NBS II b. WWVB-N.R.C.
$(M_4\text{-NBS II})_{av} = +1.1 \times 10^{-10}$ 106—Boulder 112—Cruft 109—WWV 110—NRL	91	a. WWV-106 b. 106-NBS II c. WWV-110 d. WWV-112 e. WWV-109

[a] Data of Nov. 30, 1959 to June 30, 1960.

Discussions of the various frequency standards involved in these comparisons will be found in the published and unpublished literature (United Kingdom Frequency Standard, *2, 34, 40, 41, 43;* Canadian Frequency Standard, *3, 44;* The Atomichron, *27, 34, 40, 41;* The United States Frequency Standard, *1, 32, 33, 42*).

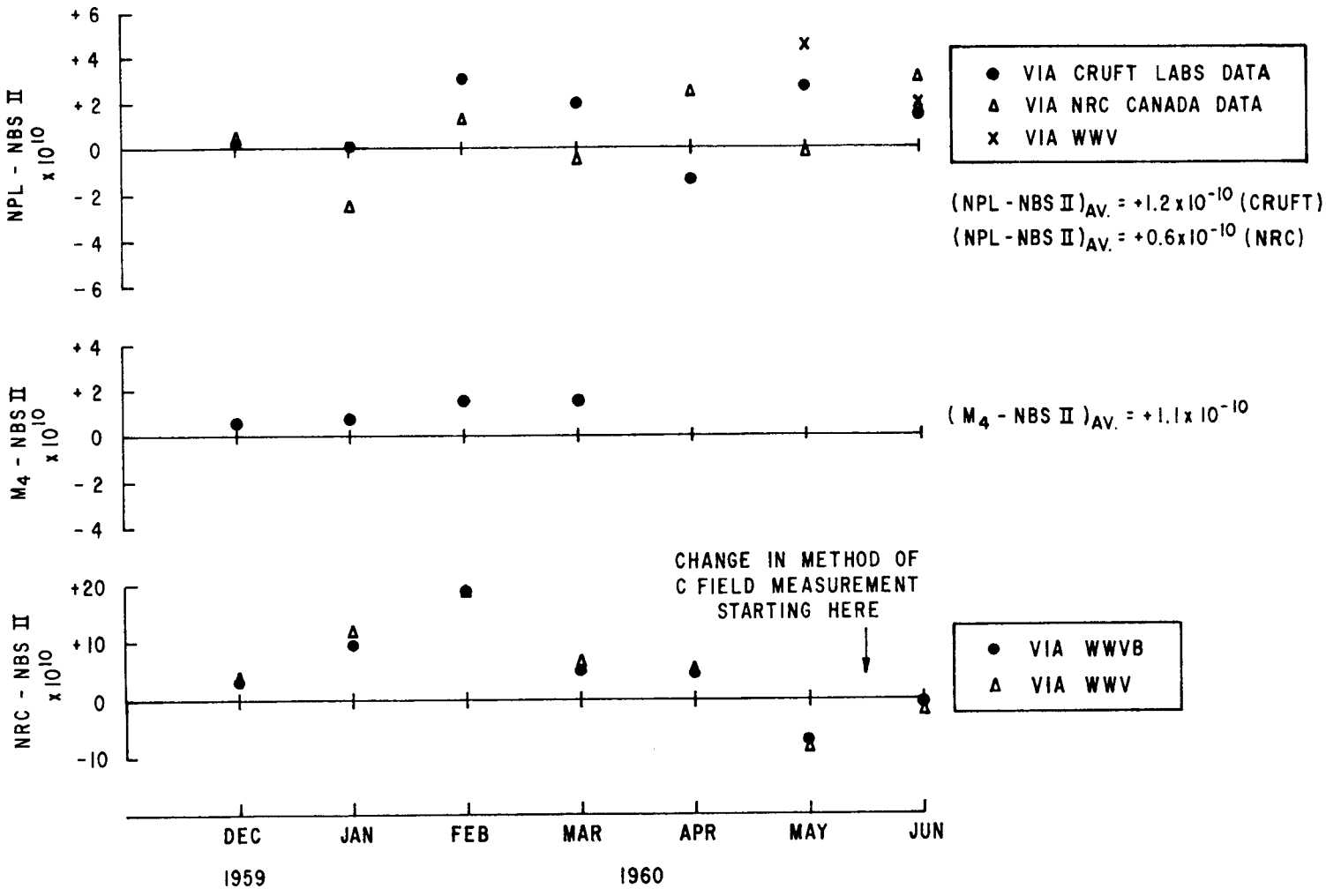

FIG. 28. Comparison of the United States Frequency Standard with the United Kingdom (NPL), Canadian (N. R. C.), and Atomichron standards using monthly averages.

IX. Thoughts on Future Developments

The atomic beam experiments that were carried on at the National Bureau of Standards demonstrate that beam devices of rather modest length (55 cm between the oscillating fields) can have a precision of 2×10^{-12} for measuring times the order of one hour. This is an order of magnitude better than the accuracy of these same machines. The limitation on the accuracy results from inadequate shielding and nonuniformity of the C field, and cannot be alleviated by narrowing the resonance line width. It appears that improvements in the C field would allow accuracies of 2×10^{-12} in these short beam devices. Until sufficiently uniform and permanent fields can be constructed, longer machines have limited usefulness insofar as accuracy is concerned. It does seem likely, however, that these developments will come about. Two long machines have been already put into operation. Essen and his group at NPL have an operating beam with the oscillating fields separated by 2.8 meters and a line width of about 50 cps. (*45*). The first estimate of accuracy was $1\text{–}2 \times 10^{-10}$ which was limited by the C field. Improvements in the magnetic shielding should yield higher accuracy.

Bonanomi and his group at Neuchâtel have a cesium beam with a 4-meter separation of the oscillating fields and a resonance line width of about 27 cps (*4*, *46*). Two long resonant cavities provide the two oscillating fields. In this way the Rabi pedestal is narrower and overlap errors should be smaller. Weaker C fields can be used, thus reducing the frequency uncertainty resulting from uncertainties in the C field. One disadvantage of this type of Ramsey structure is that it will likely be more difficult to measure phase shift errors. No estimate of the accuracy of this machine has been reported.

A. A Thallium Atomic Beam

Thallium-205 has been suggested by P. Kusch as a possible replacement for cesium in atomic beam standards (*47*). In view of the C field difficulties observed in the cesium standard, thallium is particularly attractive because it is much less field sensitive than is cesium.

The frequency of the field insensitive transition, $(F = 1, m_F = 0) \leftrightarrow (F = 0, m_F = 0)$, is given by

$$\nu(\mathrm{Tl}^{205}) = \nu_0(\mathrm{Tl}^{205}) + 20.4H_0^2, \tag{82}$$

where $\nu_0(\mathrm{Tl}^{205})$ is 21,310.835 ± .005 Mc (*48*). This is to be compared with

$$\nu(\mathrm{Cs}) = \nu_0(\mathrm{Cs}) + 427H_0^2$$

for the frequency of the field insensitive line of cesium. Thallium is 1/50th as sensitive to the magnetic field as cesium. Thallium has other advantages:

(a) The hfs separation ν_0 is more than twice that of cesium.

(b) There is a single σ-transition in thallium; there are seven in cesium. Frequency shifts due to overlap should be much less troublesome and a lower intensity C field can be used.

(c) There are only four states in the hfs of thallium (Fig. 29); there are 16 in cesium. Each thallium state, therefore, will have a higher population than the individual states of cesium. Higher signal intensities would then be observed for thallium if the detector efficiency were the same as for

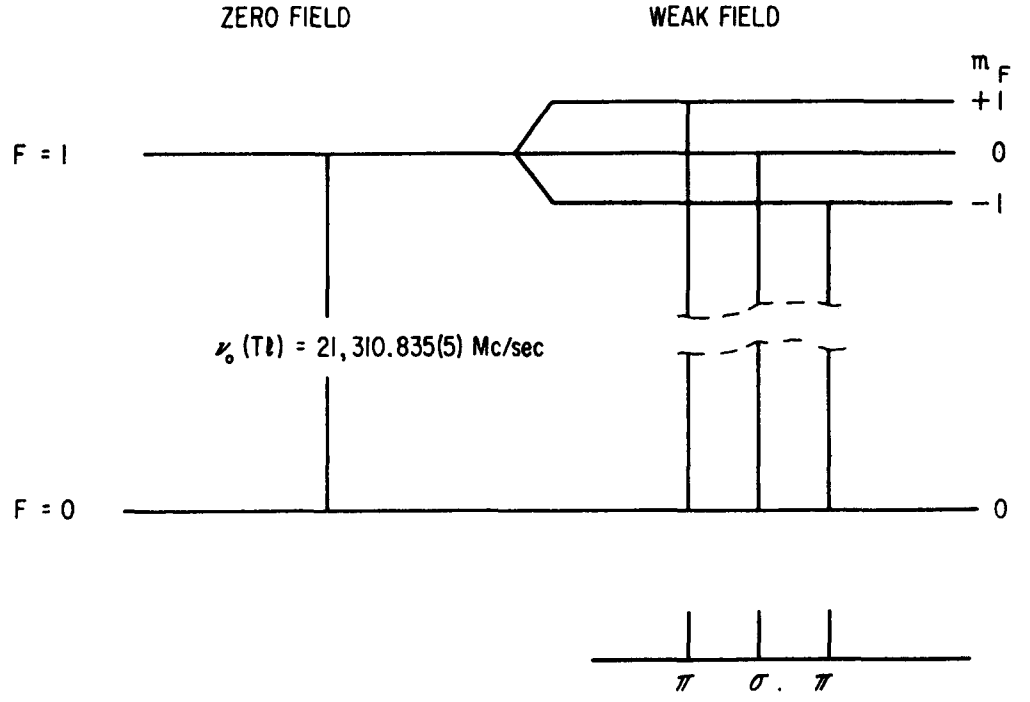

FIG. 29. The hyperfine structure of thallium (205) in the ground $^2P_{1/2}$ electronic state. $I = 1/2$.

cesium, which it is not. Thallium has the disadvantage that the method of detection is somewhat more difficult than the simpler method used for cesium. The relative efficiency must be determined experimentally before it can be said which atom will produce the better standard.

Both the National Bureau of Standards and the National Research Council of Canada are building thallium beams at the time of writing.

B. The Alkali Vapor Cell (49)

The alkali vapor frequency standard shows considerable promise although it has the disadvantage of inherent frequency shifts due to the buffer gases. These shifts are not sufficiently well understood to be treated

analytically; consequently certain recipes in construction would have to be prescribed if they were used as primary standards. Line breadths of 30 cps are attainable with much simpler apparatus than an atomic beam. Gas cell devices have been demonstrated by P. L. Bender and E. C. Beaty to have a frequency stability of 1×10^{-11} over a period of 1 month (*50*). A qualitative description of the operation of one of these devices follows.

Light from a rubidium-87 discharge is made incident upon a glass bulb containing Rb^{87} at a partial pressure of about 10^{-6} mm Hg. The bulb is contained within a resonant cavity tuned to the Rb^{87} hyperfine transition at 6835 Mc. The light radiation of interest from the lamp is the emission from the $5^2P_{3/2}$ and $5^2P_{1/2}$ states to the $5^2S_{1/2}$ ground state. By interposing a Rb^{85} absorption cell between the light source and the cavity, the light from one of the hfs lines emitted from the lamp (line *a* in Fig. 30b) can be subdued. Thus the Rb^{87} in the cavity cell will preferentially absorb b light. (The hfs of the optical radiation from both the $^2P_{1/2}$ and $^2P_{3/2}$ states will be about the same since the hfs intervals in the excited states are much less than in the ground state. The picture shown in Fig. 30b applies to both the $^2S_{1/2} \leftrightarrow {}^2P_{1/2}$ and $^2S_{1/2} \leftrightarrow {}^2P_{3/2}$ transitions.)

After excitation from the ground state to the excited states, rapid spontaneous decay back to the ground state occurs to both the $F = 2$ and $F = 1$ states with similar rates. An excess of population is accumulated in the $F = 2$ state since atoms are preferentially excited from the $F = 1$ state because of the Rb^{85} filter cell. Thus when the lamp is first switched on, the gas contained within the cavity is in thermal equilibrium and absorbs most strongly. After a time the population of the $F = 1$ state is depleted by the optical "pumping" of atoms out of this state and their subsequent accumulation in the $F = 2$ state. The gas cell becomes more transparent as indicated by an increased signal from the photo cell. If now microwave radiation of frequency 6835 Mc is applied to the cell, atoms will "flow" from the $F = 2$ state to the $F = 1$ state making more atoms available for excitation to the excited states. At this point the cell absorbs more of the incident light and a decrease in the photocell signal results. If the microwave radiation is swept through the 6835 Mc resonance the line shape may be recorded from the output of the photocell.

The inert buffer gas serves the purpose of prolonging the lifetime of the alkali metal atom in its $^2S_{1/2}$ ground state. In this state, the atoms can have many collisions with atoms of the inert buffer gas before having transitions induced between the $F = 2$ and $F = 1$ states by these collisions. Thus the lifetime of the atomic states will be prolonged by the collision processes. Collisions between the alkali atoms and the walls of the container will induce transitions, but the frequency of these collisions is drastically

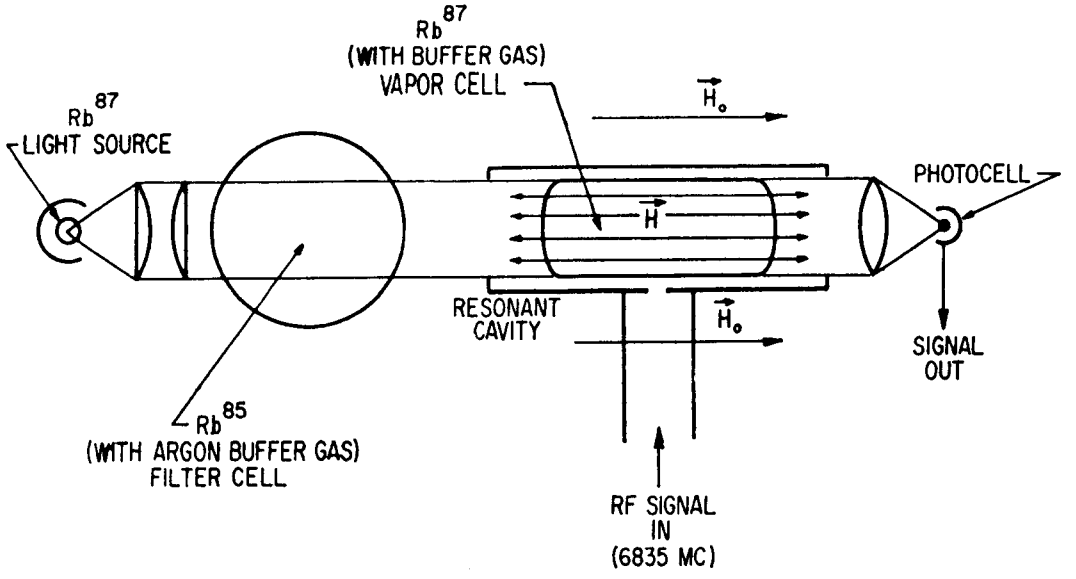

a

FIG. 30a. Rubidium-87 vapor cell. The hfs transition at 6835 Mc is observed by a change in intensity of the optical radiation transmitted through the vapor cell.

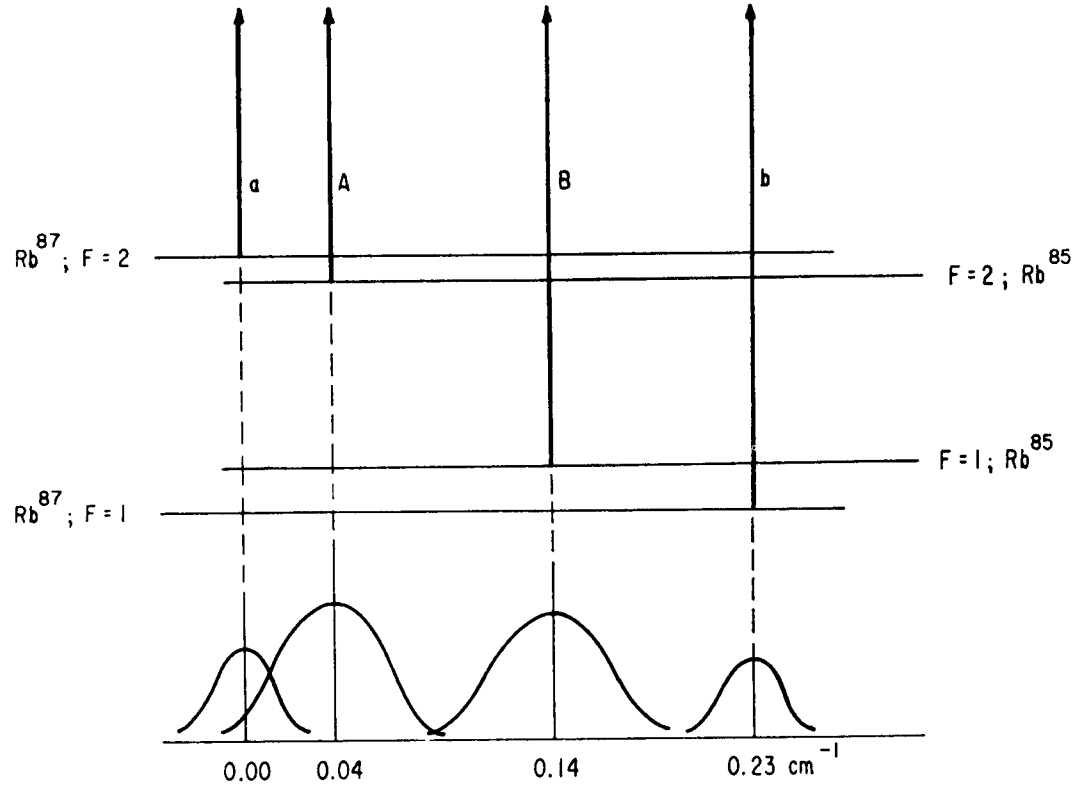

b

FIG. 30b. The filter action of the rubidium-85 bulb results from the overlap of lines a and A in the figure.

reduced by the presence of the relatively high pressure buffer gas. Doppler broadening is very small because the recoil momentum given to the radiating system by the emitted photons is distributed throughout the buffer gas via the many collisions that take place in the decay time (*51*, *52*). This "collision narrowing" is similar to the Mössbauer effect in which recoil-free gamma radiation is emitted by Fe^{57}, for example.

C. Molecular Beam Electric Resonance (53)

V. W. Hughes has suggested the $(J = 0) \leftrightarrow (J = 1)$ transition of Li^6F occurring at about 100 kMc as a frequency standard. It would employ the electric resonance beam technique which is similar to the atomic beam magnetic resonance technique. In electric resonance experiments deflections are produced through forces on the electric dipole moment in nonuniform electric fields. Electric dipole transitions are ordinarily observed. The molecular spectrum provides a much wider choice of frequencies and makes available much higher frequencies for use as a standard; higher frequencies will provide higher precision for a given signal-to-noise ratio. The molecules are distributed over a greater number of states than atoms in their ground state. Consequently, signal intensities will be substantially less. Signal intensities will generally be lower in electric resonance experiments than in a cesium beam experiment. This appears to be the primary drawback of the electric resonance method.

D. Masers

The ammonia maser has had considerable development as an extremely stable oscillator. An ammonia maser is used to stabilize the crystal oscillator driving the NBS cesium standards as mentioned previously (see Fig. 25). The measured stability for $N^{14}H_3$ masers is a few parts in 10^{12} for periods of a few minutes and about 2×10^{-11} for periods of several hours (*54*). The reproducibility of the $N^{14}H_3$ maser frequency is 2×10^{-10} (*55*). The best reproducibility, 3×10^{-11}, has been obtained using N^{15} ammonia by Bonanomi and his group (*4*). Ammonia containing N^{15} has the important advantage that the (3.3) line is single and not composed of a group of lines as is the (3.3) line of N^{14} ammonia. The relative intensities of the members of this group of lines will change with changes in the focusing voltage or beam intensity; this will cause a shift in frequency since this hfs is not resolved.[12]

Although the ammonia maser has good reproducibility for a given machine, it would probably be quite difficult to build other machines that

[12] Recently Barnes and Allan at NBS have obtained a reproducibility of 3×10^{-11} for N^{14} ammonia. They employ a servo system that continuously tunes the cavity to resonance. It uses Zeeman modulation to obtain the correction signal.

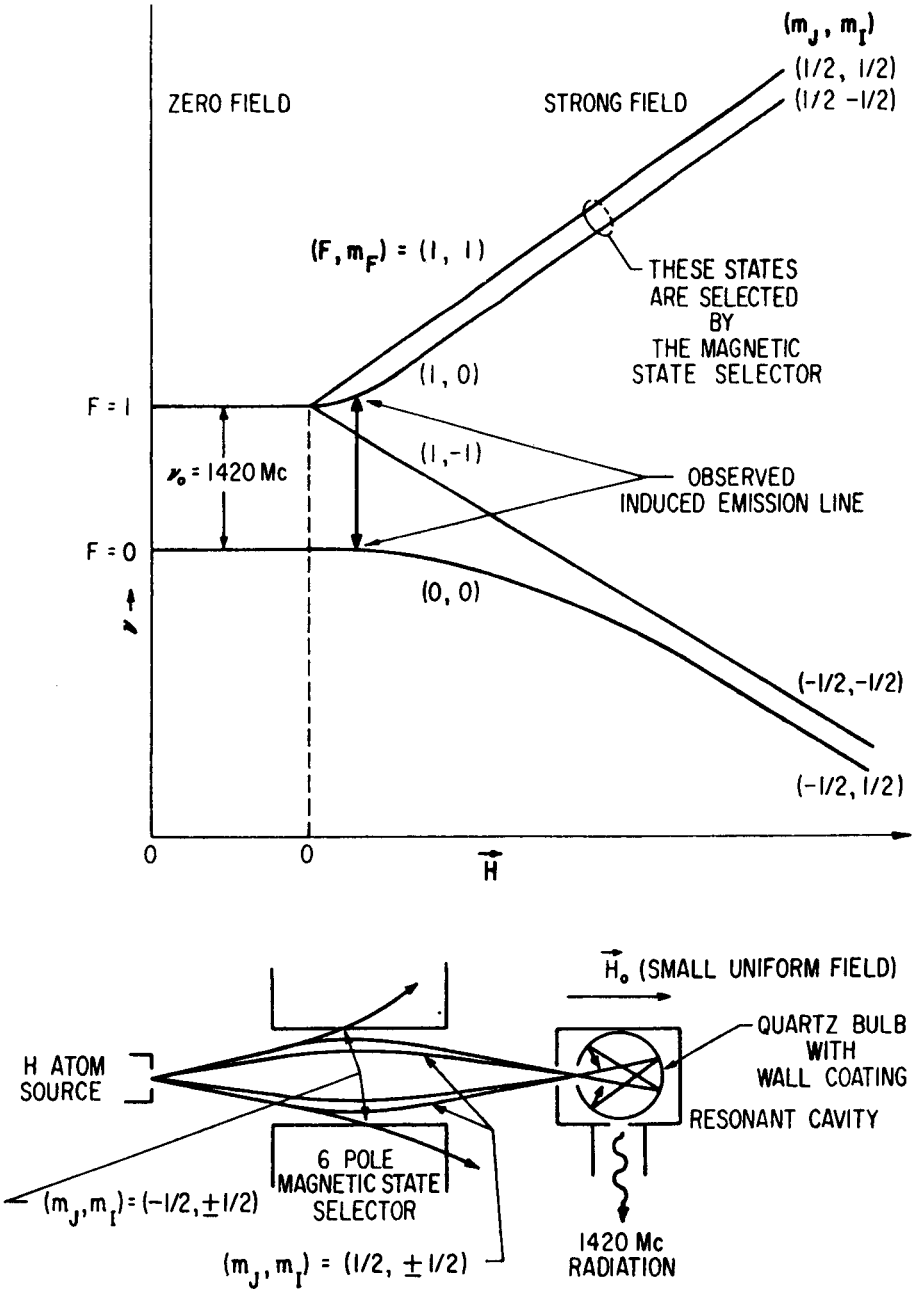

FIG. 31. The hydrogen atom beam maser.

would oscillate at frequencies closer than 1×10^{-9}. This places a rather severe limitation on its use as a primary standard. There are a number of parameters that must be carefully controlled. Furthermore, the Doppler shift cannot be precisely determined. The basic difficulty is that the frequency of the maser cannot be simply related to the Bohr frequency as it

can be for a cesium beam and the various parameters effecting the frequency require more delicate control. Other beam masers are being built to operate at higher frequencies (88 kMc, for example) by a number of laboratories, including NBS (*56*, *57*, *58*). These devices employ a Fabry-Perot interferometer as the resonator. Considerable progress has been made recently in the development of such resonators at millimeter wavelengths. Q's exceeding 100,000 are attainable (see the chapter entitled "Millimeter Wave Techniques," by W. Culshaw, in this volume).

Most recently Ramsey and his group at Harvard have succeeded in building a hydrogen atom maser (*59*) (Fig. 31). In this device hydrogen is dissociated in a discharge tube. A beam of hydrogen atoms effuses from the discharge tube and passes through a magnetic state selector. Atoms in the $F = 2, m_F = 1,0$ states are focused into a quartz bulb contained within a resonant cavity tuned to 1420 Mc, the hfs separation. The quartz bulb is coated with an inert, involatile film. Hydrogen atoms striking this film do not change their state—at least, not with a high probability. The atoms may have many wall collisions during the process of emission to the $F = 1$, $m_F = 0$ state. As a consequence of the long storage time in the cavity ($\sim$0.3 sec) by virtue of the wall collisions, the resonance line width (without regeneration) is about 1 cps.

The hydrogen beam maser differs significantly from the ammonia beam maser in two important ways: (a) The transitions are magnetic dipole transitions. (b) The radiating particles are retained in the resonating structure by wall collisions instead of passing directly through. It appears that this hydrogen maser is capable of higher stability than the ammonia maser because of its very narrow resonance width. However, there may be frequency shifts due to the wall collisions and perhaps some aging processes associated with the wall coatings.

Zero field solid state masers have been suggested by Bloembergen (*60*). Although such devices may provide highly stable oscillations, it is not certain how reproducible the frequency would be.

Acknowledgments

The author wishes to acknowledge the help of the various members of the Atomic Frequency and Time Standards Section of the National Bureau of Standards in the preparation of the manuscript.

The contributions of Messrs. Roger Beehler and James Barnes and Mrs. Mildred Beebe are of especial importance.

I wish to extend my gratitude to Drs. Peter Bender, William Culshaw, J. Holloway, L. Essen, J. Bonanomi, and Messrs. J. V. L. Parry, and P. Kartaschoff for many helpful discussions.

APPENDIX

The NBS Atomic Beam Frequency Standards Functional Data

	NBS-I	NBS-II
I. General dimensions (see Fig. 8b)		
l_1	11.5 cm	16.5 cm
l_2	5.1 cm	10.2 cm
l_3	46.0 cm	100.0 cm
l_4	46.0 cm	100.0 cm
l_5	5.1 cm	10.2 cm
l_6	11.5 cm	16.5 cm
II. Oven (adjustable)		
Temperature	150°C	150°C
Heater material	Nichrome	Nichrome
Heater current	0.8 amp	0.8 amp
Heater coil resistance (cold)	7 ohms	7 ohms
Slit dimensions	0.003 × 0.038 × 0.100 in.	0.015 × 0.100 × 0.187 in. (channeled)
III. Deflecting magnets (adjustable)		
Length	2.0 in.	4.0 in.
Gap width	0.040 in.	0.120 in.
Radius of convex pole piece, a (See Fig. 13.)	0.040 in.	0.120 in.
Radius of concave pole piece, b (See Fig. 13.)	0.050 in.	0.150 in.
Number of turns	200/magnet #22 wire	440/magnet #14 wire
Resistance of windings (cold)	2 ohms	1.6 ohms
Typical magnet current	1.4 amp	2–3 amp
Stern-Gerlach peak separation, each magnet	0.006 in.	0.040 in.
Power dissipation, each magnet	4 watts	5–14 watts
IV. Detector (adjustable)		
Material	80% Pt–20% Ir	80% Pt–20% Ir
Width	0.005 in.	0.015 in.
Current	0.6 amp	0.6 amp
Temperature	820°C	820°C
V. Center collimating slit (adjustable)		
Material	Plastic, brass, or aluminum	Plastic, brass, or aluminum
Width	0.003 in.	0.015 in.
VI. Resonant cavity		
Principle mode	$TE_{0,1,60}$	$TE_{0,1,100}$
Dimensions of beam holes	$\frac{1}{16} \times \frac{3}{16}$ in.	$\frac{1}{16} \times \frac{3}{16}$ in.
Coupling hole diameter	0.312 in.	0.328 in.
Loaded Q	~7000	~5500
Tuning range with adjustable probe opposite coupling hole	0.9 Mc	1.8 Mc
Separation of ends	56 cm	163 cm

463-550 O - 72 - 6

References

1. Mockler, R. C., Beehler, R. E., and Snider, C. S., *IRE Trans. on Instrumentation*, **I-9**, 120 (1960).
2. Essen, L., and Parry, J. V. L., *Phil. Trans. Roy. Soc.* **A250**, 45 (1957).
3. Kalra, S. N., Bailey, R., and Daams, H., *Nature* **183**, 575 (1959).
4. De Prins, J., and Kartaschoff, P., "Applications de la spectroscopie hertzienne à la mésure de frequences et du temps." Lab. suisse recherches horlogeres, Neuchâtel, Switzerland, 1960.
5. Markowitz, W., Hall, R. G., Essen, L., and Parry, J. V. L., *Phys. Rev. Letters* **1**, 105 (1958).
6. Kusch, P., and Hughes, V. W., *in* "Handbuch der Physik" (S. Flügge, ed.), Vol. 37, Part I, pp. 1–172. Springer, Berlin, 1959.
7. Ramsey, N. F., "Molecular Beams." Oxford Univ. Press, London and New York, 1956.
8. Kopfermann, H., "Nuclear Moments" (E. E. Schneider, ed. and transl.), Pure and Appl. Phys. Ser., Vol. 2. Academic Press, New York, 1948.
9. Bethe, H. A., and Salpeter, E. E., "Quantum Mechanics of One- and Two-Electron Atoms." Academic Press, New York, 1957.
10. Kusch, P., *Phys. Rev.* **100**, 1188 (1955); Wittke, J. P., and Dicke, R. H., *ibid.* **103**, 620 (1956); Anderson, L. W., Pipkin, F. M., and Baird, J. C., Jr., *Phys. Rev. Letters* **4**, 69 (1960).
11. Salwen, H., *Phys. Rev.* **101**, 623 (1956).
12. Breit, G., and Rabi, I. I., *Phys. Rev.* **38**, 2082 (1931).
13. King, J. G., and Zacharias, J. R., *Advances in Electronics and Electron Phys.* **8**, 1–83 (1956).
14. Friedburg, H., and Paul, W., *Naturwissenschaften* **38**, 159 (1951); Friedburg, H., *Z. Physik.* **130**, 493 (1951).
15. Lemonick, A., and Pipkin, F. M., *Phys. Rev.* **95**, 1356 (1954). Lemonick, A., Pipkin, F. M., and Hamilton, D. R., *Rev. Sci. Instr.* **26**, 1112 (1955).
16. Gordon, J. P., Zeiger, H. J., and Townes, C. H., *Phys. Rev.* **99**, 1264 (1955).
17. Zandburg, É. Ya., and Ionov, N. I., *Uspehki Fiz. Nauk* **57**, 581 (1959); English translation in *Soviet Phys.—Uspehki* **67**(2), 255 (1959).
18. Varnerin, L. J., Jr., *Phys. Rev.* **91**, 859 (1953).
19. Van der Ziel, A., *Physica* **9**, 177 (1942).
20. Strutt, M. J. O., and Van der Ziel, A., *Physica* **9**, 513 (1942).
21. Schockley, W., and Pierce, J. R., *Proc. IRE* **26**, 321 (1938).
22. Allen, J. S., *Proc. IRE* **38**, 346 (1950).
23. Daly, R. T., Ph. D. Thesis, Phys. Dept. Mass. Inst. Technol., Cambridge, Mass. (1954), unpublished.
24. Zacharias, J. R., Yates, J. G., and Haun, R. D., Mass. Inst. Technol., Research Lab. Electronics Quart. Progr. Rept. No.35 (1954), unpublished.
25. Milatz, J. M. W., and Bloembergen, N., *Physica* **11**, 449 (1946).
26. Polevsky, H., Swank, R. K., and Grenchik, R., *Rev. Sci. Instr.* **18**, 298 (1947).
27. "Instruction Manual for Atomichron Model NC-1001." National Company, Inc., Malden, Mass. 1957.
28. Condon, E. U., and Shortley, G. H., "Theory of Atomic Spectra," pp. 63–66. Cambridge Univ. Press, London and New York, 1951.
29. Torrey, H. C., *Phys. Rev.* **59**, 293 (1941).
30. Salwen, H., *Phys. Rev.* **99**, 1274 (1955).

31. Bloch, F., and Siegert, A., *Phys. Rev.* **57,** 522 (1940).
32. Mockler, R. C., Beehler, R. E., and Barnes, J. A., *in* "Quantum Electronics: A Symposium" (C. H. Townes, ed.) pp. 127–145. Columbia Univ. Press, New York, 1960.
33. Beehler, R. E., Mockler, R. C., and Snider, C. S., *Nature* **187,** 681 (1960).
34. Holloway, J., Mainberger, W., Reder, F. H., Winkler, G. M. R., Essen, L., and Parry, J. V. L., *Proc. IRE* **47,** 1730 (1959).
35. Black, H. S., "Modulation Theory," pp. 195–200. Van Nostrand, New York, 1953.
36. Barnes, J. A., and Heim, L. E., A high resolution ammonia maser spectrum analyser. *IRE Trans. on Instrumentation,* to be published.
37. Barnes, J. A., and Mockler, R. C., *IRE Trans. on Instrumentation* **I-9,** 149 (1960).
38. Ramsey, N. F., *in* "Recent Research in Molecular Beams" (I. Estermann, ed.), p. 107. Academic Press, New York, 1959. Ramsey, N. F., *Phys. Rev.* **100,** 1191 (1955).
39. Haun, R. D., Jr., and Zacharias, J. R., *Phys. Rev.* **107,** 107 (1957).
40. Essen, L., Parry, J. V. L., Holloway, J. H., Mainberger, W. A., Reder, F. H., and Winkler, G. M. R., *Nature* **182,** 41 (1958).
41. McCoubry, A. O., *IRE Trans. on Instrumentation* **I-7,** 203 (1958).
42. Schafer, G. E., and Salazar, H. F., A simple multiplier chain for excitation of cesium beam resonators. Natl. Bur. Standards (U.S.) report (1960), unpublished.
43. Essen, L., and Parry, J. V. L., *Proc. Inst. Elec. Engrs. (London), Pt. B* **106,** 240 (1959).
44. Kalra, S. N., and Bailey, R., *in* "Quantum Electronics: A Symposium" (C. H. Townes, ed.), pp. 121–126. Columbia Univ. Press, New York, 1960.
45. Essen, L., and Parry, J. V. L., *Nature* **184,** 1791 (1959).
46. Kartaschoff, P., Bonanomi, J., and De Prins, J., U. S. Army Signal Research and Development Lab., Ft. Monmouth, New Jersey, Proc. 14th Ann. Frequency Control Symposium (1960), pp. 354–360, unpublished.
47. Kusch, P., U. S. Army Signal Research and Development Lab., Ft. Monmouth, New Jersey, Proc. 11th Ann. Frequency Control Symposium, pp. 373–384 (1957), unpublished.
48. Lurio, A., and Prodell, A. G., *Phys. Rev.* **101,** 79 (1956).
49. Bender, P. L., *in* "Quantum Electronics: A Symposium" (C. H. Townes, ed.), pp. 110–121. Columbia Univ. Press, New York, 1960.
50. Carpenter, R. J., Beaty, E. C., Bender, P. L., Saito, S., and Stone, R. O., *IRE Trans. on Instrumentation* **I-9,** 132 (1960).
51. Dicke, R. H., *Phys. Rev.* **89,** 472 (1953).
52. Wittke, J. P., and Dicke, R. H., *Phys. Rev.* **103,** 620 (1956)
53. Hughes, V. W., *Rev. Sci. Instr.* **30,** 689 (1959).
54. Mockler, R. C., and Barnes, J. A., U. S. Army Signal Research and Development Lab., Ft. Monmouth, New Jersey, Proc. 13th Ann. Frequency Control Symposium, pp. 583–595 (1959), unpublished; Bonanomi, J., and Herrmann, J., *Helv. Phys. Acta* **29,** 224 and 451 (1956); Bonanomi, J., De Prins, J., Herrmann, J., and Karatschoff, P., *ibid.* p. 228; **30,** 492 (1957); Bonanomi, J., De Prins, J., and Herrmann, J., *ibid.* **31,** 282 (1958); Bonanomi, J., Herrmann, J., De Prins, J., and Kartaschoff, P., *Rev. Sci. Instr.* **28,** 879 (1957).
55. Mockler, R. C., Barnes, J. A., Beehler, R. E., and Fey, R. L., *IRE Trans. on Instrumentation* **I-7,** 201 (1958).
56. Gallagher, J. J., U. S. Army Signal Research and Development Laboratory, Ft.

Monmouth, New Jersey, Proc. 13th Ann. Frequency Control Symposium, pp. 604–617 (1959), unpublished.
57. Barnes, F. S., *in* "Quantum Electronics: A Symposium" (C. H. Townes, ed.), p. 57. Columbia Univ. Press, New York, 1960.
58. Culshaw, W., and Mockler, R. C., A Fabry-Perot maser. Natl. Bur. Standards (U.S.) report (1959), unpublished.
59. Goldenberg, H. M., Kleppner, D., and Ramsey, N. F., *Phys. Rev. Letters* **5**, 361 (1960).
60. Bloembergen, N., *in* "Quantum Electronics: A Symposium" (C. H. Townes, ed.), p. 160. Columbia Univ. Press, New York, 1960.